



Degradation of Adenine on the Martian Surface in the Presence of Perchlorates and Ionizing Radiation: A Reflectron Time-of-flight Mass Spectrometric Study

Sándor Góbi^{1,2}, Alexandre Bergantini^{1,2}, and Ralf I. Kaiser^{1,2}

¹ Department of Chemistry, University of Hawaii at Mānoa, Honolulu, HI 96822, USA

² W.M. Keck Laboratory in Astrochemistry, University of Hawaii at Mānoa, Honolulu, HI 96822, USA; ralfk@hawaii.edu

Received 2016 December 22; revised 2017 March 2; accepted 2017 March 5; published 2017 March 29

Abstract

The aim of the present work is to unravel the radiolytic decomposition of adenine ($C_5H_5N_5$) under conditions relevant to the Martian surface. Being the fundamental building block of (deoxy)ribonucleic acids, the possibility of survival of this biomolecule on the Martian surface is of primary importance to the astrobiology community. Here, neat adenine and adenine–magnesium perchlorate mixtures were prepared and irradiated with energetic electrons that simulate the secondary electrons originating from the interaction of the galactic cosmic rays with the Martian surface. Perchlorates were added to the samples since they are abundant—and therefore relevant oxidizers on the surface of Mars—and they have been previously shown to facilitate the radiolysis of organics such as glycine. The degradation of the samples were monitored *in situ* via Fourier transformation infrared spectroscopy and the electron ionization quadrupole mass spectrometric method; temperature-programmed desorption profiles were then collected by means of the state-of-the-art single photon photoionization reflectron time-of-flight mass spectrometry (PI-ReTOF-MS), allowing for the detection of the species subliming from the sample. The results showed that perchlorates do increase the destruction rate of adenine by opening alternative reaction channels, including the concurrent radiolysis/oxidation of the sample. This new pathway provides a plethora of different radiolysis products that were identified for the first time. These are carbon dioxide (CO_2), isocyanic acid ($HNCO$), isocyanate (OCN^-), carbon monoxide (CO), and nitrogen monoxide (NO); an oxidation product containing carbonyl groups ($R_1R_2-C=O$) with a constrained five-membered cyclic structure could also be observed. Cyanamide ($H_2N-C\equiv N$) was detected in both irradiated samples as well.

Key words: astrochemistry – methods: laboratory: solid state – planets and satellites: surfaces – techniques: spectroscopic

1. Introduction

During the past decades, attempts to untangle the chemical fate of organics on the Martian surface have been of primary importance to the planetary science and astrobiology communities. Organic compounds might accumulate on the surface of Mars owing to two different sources: *in situ* formation (Orgel 2004; Cleaves et al. 2006; Roy et al. 2007; ten Kate 2010) and/or delivery via interplanetary dust particles (Flynn 1996; Moores & Schuerger 2012) and by meteoritic infall (Botta & Bada 2002; Callahan et al. 2011; Pearce & Pudritz 2016). However, after their deposition to the surface, these organics are continuously exposed to energetic solar photons and galactic cosmic rays (GCRs), leading to their radiolytic destruction. Having a subtle atmosphere with an average pressure of 7 mbar (Armstrong et al. 2004), Mars also lacks a magnetic field (Acuña et al. 1999), allowing energetic GCR particles to reach the Martian surface. Previously, the effect of GCRs has generally been neglected as their energy flux is six orders of magnitude lower than the flux of solar UV photons (Molina-Cuberos et al. 2001; Cockell & Raven 2004; Dartnell et al. 2007). Liquid water that might be present in the shallow subsurface (1–3 cm) in the form of thin films that remain stable even below the freezing point of bulk water (Shivak & Pavlov 2012; Keresztsuri & Góbi 2014) may also facilitate the destruction of organics with a half-life of $\geq 10^6$ years at 273 K via hydrolysis. Nonetheless, photons are effectively absorbed in the upper few tens of nanometers of the dust particles (Muñoz-Caro et al. 2006), while GCRs can penetrate the first few meters of the Martian soil (Pavlov et al. 2012). This makes

GCRs the primary candidate that accounts for the destruction of organics in the deeper subsurface of Mars. When the calculated destruction rates of organics are compared to the rates of continuous exogenous delivery, it has been concluded that organics should still be present (Turner et al. 2016). However, according to the recent findings from the Curiosity Rover, the concentration of indigenous organics is orders of magnitude lower than expected (in the ppb region; Freissinet et al. 2015; Miller et al. 2016), implicating the presence of active oxidation agent(s) that effectively facilitate(s) the radiolytic decomposition of organics (Lasne et al. 2016). These conclusions were also supported by a Surface Enhanced Raman Scattering study that could not detect nucleobases in the Martian meteorite RBT 04262 even in trace amounts (Callahan et al. 2013). The role of oxidizers in the radiolytic decay of organic compounds on the Martian surface/subsurface is the most widely accepted explanation and was proposed based on the results of the Viking (Biemann et al. 1976; Biemann & Bada 2011) and Phoenix Landers (Sutter et al. 2009) along with the data obtained by the Curiosity Rover (Leshin et al. 2013; Ming et al. 2014). Perchlorates (ClO_4^-) are considered to be the most effective oxidants (Hecht et al. 2009; Glavin et al. 2013), with concentrations that can be as high as 1.0% by weight (Davila et al. 2013). They are likely formed via heterogeneous photochemical (Smith et al. 2014), photocatalytic (Carrier & Kounaves 2015), or radiation-induced surface reactions within carbon dioxide (CO_2)-bearing ices (Kim et al. 2013; Wilson et al. 2016).

Numerous studies have attempted to explain the scarcity of organic compounds on the Martian surface by investigating

their radiolytic destruction under simulated Martian conditions. Among these organics, nucleobases—the fundamental building blocks of ribonucleic acid (RNA) and deoxyribonucleic acid (DNA)—have also been the focus of interest in the past decades, resulting in laboratory experiments carried out with adenine ($C_5H_5N_5$) samples (Table 1). Adenine—formally the pentamer of the hydrogen cyanide (HCN) molecule—is known to be resistant against energetic irradiation as it can undergo rapid radiationless deactivation involving conical intersections from its excited states accessed via the $n\pi^*$ transition (Perun et al. 2005; Barbatti et al. 2015; Impronta et al. 2016), making its lack of detection on Mars especially intriguing. An early work on the radiolysis of organics was carried out by Oró & Holzer (1979). The authors found that the presence of oxygen greatly increases the destruction rate of the organic compounds adenine ($C_5H_5N_5$), glycine (H_2NCH_2COOH), and naphthalene ($C_{10}H_8$). These organic samples did not show any change when irradiated by broadband UV photons (200–300 nm). However, under oxygen-rich atmospheres, 99% of the sample molecules were destroyed using the same irradiation doses. The authors eventually concluded that the combined effect of energetic irradiation and the presence of oxidants are both fundamentally necessary for the degradation of organic molecules on Mars. Guan et al. (2010) probed the photostability of several organics—glycine (H_2NCH_2COOH), xanthine ($C_5H_4N_4O_2$), hypoxanthine ($C_5H_4N_4O$), adenine ($C_5H_5N_5$), guanine ($C_5H_5N_5O$), urea ($(H_2N)_2-C=O$), carbon suboxide polymer ($(C_3O_2)_n$), and HNC polymer ($(HCN)_n$)—during the ESA BIOPAN 6 mission. Their half-lives ranged from a few days to a few tens of days for the most photo-resistant molecules (adenine, guanine, hypoxanthine). Fifteen powdered organic compounds were radiolyzed by 200–280 nm UV-C photons in the work of Schuerger et al. (2011) when they examined the evolution of methane (CH_4) upon irradiation under inert and Mars-analog atmospheres. They found that 1 g of adenine ($C_5H_5N_5$) yields a moderate amount of 0.040 nmol of methane (CH_4) after 1 hr of irradiation. Thin layers of nucleobases adsorbed on magnesium oxide (MgO) and forsterite (Mg-rich end-member of olivine, Mg_2SiO_4) were also investigated (Fornaro et al. 2013), and the results confirmed the high intrinsic photostability of such molecules. Although molecular destruction seemed to occur on both surfaces for uracil ($C_4H_4N_2O_2$), this was in contrast to the behavior of the other three studied molecules. The UV irradiation caused only the excitation of the adenine ($C_5H_5N_5$) vibrations, whereas cytosine ($C_4H_5N_3O$) and hypoxanthine ($C_5H_4N_4O$) proved to be even more photo-resistant. Nevertheless, according to their results, magnesium oxide (MgO) and forsterite (Mg_2SiO_4) surfaces have no protective effect against UV irradiation; they may even have a catalytic effect on the degradation. The decomposition rate of thin films of adenine ($C_5H_5N_5$) on the magnesium fluoride (MgF_2) window was also determined when radiolyzed by 115–300 nm UV photons under vacuum by Saifagh et al. (2014); the irradiation products—similarly to all above-mentioned studies—were not determined. Poch et al. (2014) also investigated the UV radiolysis of thin films of adenine ($C_5H_5N_5$) under inert atmosphere, and they found evidence for the formation of amines ($-NH_2$), isocyanides ($R-N=C$), and nitriles ($R-C\equiv N$) in an extended conjugated system (like $-C=C-C=N-$). In a later work, these authors also examined the role of a silicate layer (nontronite smectite clay being the most abundant

phylllosilicate on Mars), leading to the conclusion that it does have a photo-protective effect; the destruction rates of glycine (H_2NCH_2COOH) and adenine ($C_5H_5N_5$) decreased by a factor of five (Poch et al. 2015). The only occasion when adenine samples were irradiated by energetic electrons to simulate GCRs was the work done by Evans et al. (2011). This study used neat adenine ($C_5H_5N_5$) samples and studied the effect of the radiolysis of a thin oxygen (O_2) ice deposited on the pre-irradiated adenine film as well. In the first case, formation of nitriles ($R-C\equiv N$) could be observed, whereas the irradiation of the adenine sample covered by oxygen ice yielded epoxides ($C-O-C$) and a carbonyl-bearing compound ($R_1R_2-C=O$) besides the nitriles.

There have been also efforts made to shed light on the decomposition mechanism of perchlorate samples, concluding that upon irradiation they yield atomic oxygen (O), which later quickly recombines into its molecular form (O_2 ; Turner et al. 2016), providing an oxidizing environment for the surrounding organic molecules. A later work also found an alternative pathway resulting in chlorine dioxide (ClO_2) aside from oxygen, which may further accelerate the decomposition of organics as it is an even more proficient oxidant (Góbi et al. 2016b). It has also been previously shown that two parallel decay mechanisms coexist when amino acids are irradiated in the presence of magnesium perchlorate hexahydrate ($Mg(ClO_4)_2 \cdot 6H_2O$): the radiolytic decomposition of the organic molecule by the energetic electrons *and* the oxidation of the molecule and its irradiation products by oxygen formed upon the irradiation of neighboring perchlorate units (Góbi et al. 2016a). It is important to note that the most stable form of magnesium perchlorate under Martian conditions is hexahydrate (Chevrier et al. 2009; Toner et al. 2014). Increased formation rates of oxidized products such as carbon dioxide (CO_2) confirmed the conclusion that the active oxygen originating from radiolysis of perchlorate (ClO_4^-) accounts for the elevated rates of decomposition as well. Furthermore, the detailed decomposition mechanism of glycine and the effect of the organics-perchlorate ratio were studied in a recent paper utilizing the PI-ReTOF-MS method (Góbi et al. 2017). Although these previous works unraveled the detailed mechanisms on the destruction of the simplest amino acid—glycine (H_2NCH_2COOH)—on Mars, the destruction of nucleobases in the presence of an oxidizer under conditions prevalent in Mars have never been investigated so far.

Here, we aim to detect the decomposition and oxidation products of adenine ($C_5H_5N_5$) in the absence/presence of perchlorates by means of Fourier Transformation Infrared Spectroscopy (FTIR) and state-of-the-art single photon photoionization reflectron time-of-flight mass spectrometry (PI-ReTOF-MS; Jones & Kaiser 2013; Maity et al. 2014; Tarcaj et al. 2016). PI-ReTOF-MS has the unique advantage that fragmentation of the sublimed and ionized species are negligible in almost all cases, meaning that only the parent molecular ions can be observed (Abplanalp et al. 2015; Turner et al. 2015); it is also possible to discriminate between the structural isomers of a molecular formula based on their different ionization energies (Abplanalp et al. 2015). Therefore, the present PI-ReTOF-MS study represents an ideal approach to explore and to identify the radiolytic oxidation products of adenine ($C_5H_5N_5$) exposed to energetic electrons in the presence of perchlorates.

Table 1
Summary of Previous Experimental Results of the Radiolysis of Adenine Films under Simulated Martian Conditions

Adenine Sample	Atmosphere (mbar)	Temperature (K)	Type of Radiation	Admixtures	Products	References
Absorbed on powdered quartz (SiO_2)	10^{-3} and various levels of oxygen (O_2)	<263, 298	UV, 200–300 nm	...	Not specified	Oró & Holzer 1979
Thin layers on magnesium fluoride (MgF_2) window	Not specified	251–303	Solar UV	...	Not specified	Guan et al. 2010
130 ± 14 nm thick layer on a silver (Ag) substrate	8×10^{-11} 6.9 ± 0.1 1.: Pure argon (Ar) 2.: Mars analog (95.3% CO_2) 3.: Pure nitrogen (N_2)	11.4 ± 0.3	5 keV e^-	1.:... 2.: 500 nm thick O_2 ice on top of the sample	1.: Nitriles ($\text{R}-\text{C}\equiv\text{N}$) 2.: Nitriles ($\text{R}-\text{C}\equiv\text{N}$), epoxides ($\text{C}-\text{O}-\text{C}$), carbonyl functional group ($\text{R}_1\text{R}_2-\text{C}=\text{O}$)	Evans et al. 2011
Powder	10^{-2} – 10^{-3}	293	UV-C, 200–280 nm	...	Monitoring only methane (CH_4) formation	Schuerger et al. 2011
Adsorbed on magnesium oxide (MgO) and forsterite (Mg_2SiO_4)	Not specified	UV, 185–2000 nm	...	Not specified		Fornaro et al. 2013
Thin layers on MgF_2 window	10^{-4}	Not specified	115–300 nm	...	Not specified	Saiagh et al. 2014
Thin layers on MgF_2 window	6 ± 1 , nitrogen (N_2)	218 ± 2	UV, 190–400 nm	...	Amine functional groups ($-\text{NH}_2$), isocyanides ($\text{R}-\text{N}=\text{C}$) and/or nitriles ($\text{R}-\text{C}\equiv\text{N}$) involved in an extended conjugated system (as $-\text{C}=\text{C}-\text{C}=\text{N}-$).	Poch et al. 2014
Thin layers on MgF_2 window	6 ± 1 (N_2)	218 ± 2	UV, 190–400 nm	Nontronite phyllosilicate	Same as in Poch et al. 2014	Poch et al. 2015

2. Experiment

The experiments were conducted in a contamination-free ultra-high vacuum (UHV) stainless steel chamber that can be evacuated to a base pressure of a few 10^{-11} mbar using oil-free magnetically suspended turbomolecular pumps and dry scroll backing pumps (Jones & Kaiser 2013; Maity et al. 2014; Tarczay et al. 2016). A polished silver mirror is mounted onto a cold finger made of oxygen-free high conductivity copper (OFHC) using indium foil to ensure thermal conductivity. The cold finger is cooled by a closed-cycle helium refrigerator (Sumitomo Heavy Industries, RDK-415E) while the temperature can be maintained by the help of a heater connected to a programmable temperature controller. The entire setup is freely rotatable within the horizontal center plane and translatable in the vertical axis via UHV compatible bellows and a differentially pumped rotational feedthrough. The silver mirror is used as a substrate and can be cooled down to 5.5 ± 0.1 K. It should be pointed out that this temperature is well below that of the surface of 160 to 240 K, and therefore does not represent the Martian environment. Nevertheless, these experiments serve as a proof-of-concept study to unravel the decay mechanism of adenine ($C_5H_5N_5$) as well as the formation pathways of irradiation products like isocyanic acid (HNCO) when irradiated with energetic electrons. A schematic view of the simulation chamber discussing its geometry, the relative position of the instruments, and a general description of the experimental procedure can be found in Jones & Kaiser (2013).

Films with a nominal thickness of $1\text{ }\mu\text{m}$ on the silver substrates were prepared by using pure adenine ($C_5H_5N_5$, Sigma Aldrich, 99+%) and its 1:1 mixture with magnesium perchlorate hexahydrate ($Mg(ClO_4)_2 \cdot 6H_2O$, Sigma Aldrich, 99.0+%, Table 2). By knowing the volume of the solution added onto the substrate, the average density and area of the solid sample and the average sample thicknesses could also be calculated. The samples were prepared by utilizing the method established in our previous work (Góbi et al. 2016a). Briefly, pure adenine (for the neat adenine samples) or adenine with $Mg(ClO_4)_2 \cdot 6H_2O$ in a 1:1 molar ratio (for the adenine–Mg($ClO_4)_2 \cdot 6H_2O$ 1:1 mixture samples) were dissolved in distilled water (H_2O), then 0.250–0.390 ml of these solutions (Table 2) was placed onto the surface of the silver substrates. The solvent was evaporated by heating the samples up to 323–333 K. The samples were then inserted into the main chamber; after its evacuation, the chamber was warmed up for two days to eliminate water and residual gases. It is important to point out that their temperature never exceeded 320 K, ensuring that none of the sample material is lost during this “bakeout” process. The substrates with the sample films on them were then cooled down to 5.5 ± 0.1 K and bombarded isothermally with 5 keV electrons for 3 hr at a current of 265–290 nA over an area of $1.5 \pm 0.3\text{ cm}^2$ at an angle of incidence of 70° relative to the surface normal (Table 2). The emission current was measured before and after irradiation utilizing a Faraday cup (Kimball Physics, FC-71) mounted inside the main chamber.

Based on the average electron currents, the samples were exposed to $1.79\text{--}1.95 \times 10^{14}$ electrons during the irradiation. Monte Carlo (CASINO) simulations (Drouin et al. 2007) were also performed to estimate the average dose absorbed by the molecules in the sample and were found to be 335–340 eV per adenine ($C_5H_5N_5$) molecule and 820 eV per $Mg(ClO_4)_2 \cdot 6H_2O$

molecule. These doses correspond to about six to seven hundred million years of exposure time 2–3 cm below the Martian surface (Pavlov et al. 2012). It is worth noting that the thickness of the samples of about 1100 nm was significantly larger than the calculated average penetration depth of the electrons (180–200 nm, Table 2), verifying that the electrons interacted only with the deposited sample molecules but not with the silver substrate itself. It should be emphasized that the high electron current (therefore the high dose) was needed because of the already-mentioned resistant nature of adenine ($C_5H_5N_5$) to energetic irradiations, and preliminary experiments made by Evans et al. (2011) showed that lower doses do not destroy the adenine molecule and yield the radiolysis products to a sufficient degree. A blank experiment (a sample containing only $Mg(ClO_4)_2 \cdot 6H_2O$) was also carried out in order to monitor potential contaminants.

The electron radiolysis of the samples was monitored online and in situ by means of an FTIR spectrometer (Nicolet 6700) in the range of $4000\text{--}650\text{ cm}^{-1}$ at a resolution of 4 cm^{-1} . Each spectrum was collected for two minutes, resulting in a set of 90 infrared spectra during the radiation exposure for both systems. To detect the species sublimed into the gas phase, an electron ionization quadrupole mass spectrometer (EI-QMS, Extrel Model 5221) operating in residual gas analyzer mode was utilized in the mass range of 1–100 m/z; the electron impact energy was set to 70 eV. After irradiating the sample, it was kept at 5.5 ± 0.1 K for one additional hour to make sure it reaches the state of equilibrium; then, temperature-programmed desorption (TPD) studies were conducted by warming them up to 300 K at a rate of 1.0 K min^{-1} . Once the sample reached 300 K, it was kept at this temperature for an additional 3 hr to let the irradiation products diffuse out of the sample and into the gas phase completely. During the TPD process, the subliming molecules were monitored using the PI-ReTOF-MS instrument (Jordan TOF Products Inc.; Jones & Kaiser 2013) by ionizing them via single photon ionization with coherent vacuum ultraviolet (VUV) light. Pulsed VUV light with a wavelength of 118.2 nm (10.49 eV) was generated by nonlinear four-wave mixing utilizing xenon (Xe) gas as the nonlinear medium (Hilbig & Wallenstein 1981; Maity et al. 2014). Fully detailed discussion of the PI-ReTOF-MS technique, the VUV laser generation by four-wave mixing, and applicability of this method to astrophysically relevant samples can be found in previous papers presented by our group (Maity et al. 2014; Abplanalp et al. 2015, see also their Supplementary Information and Appendix). PI-ReTOF-MS measurements of Mars-relevant samples were discussed in Góbi et al. (2017).

3. Results

3.1. Infrared Spectrum of the Adenine and Adenine–Magnesium Perchlorate Hexahydrate Samples

3.1.1. Neat Adenine Samples

The FTIR spectra of the neat adenine ($C_5H_5N_5$) and adenine–magnesium perchlorate hexahydrate ($Mg(ClO_4)_2 \cdot 6H_2O$) mixture in the range of 4000 and 650 cm^{-1} are shown in Figure 1. The assignments of adenine ($C_5H_5N_5$) vibrational modes are summarized in Table 3; these features have been well-known for decades, and our spectra of the neat adenine sample (Figure 1(a)) shows excellent agreement with those of previous works

Table 2
Summary of Adenine and Adenine–Mg(ClO₄)₂ · 6H₂O 1:1 Sample Preparation Details and the CASINO Simulations Performed on the Electron Radiolysis Experiments

	Adenine	Adenine–Mg(ClO ₄) ₂ · 6H ₂ O 1:1
Mass of adenine (g)	0.0383 ± 0.0001	0.0103 ± 0.0001
Mass of Mg(ClO ₄) ₂ · 6H ₂ O (g)	0.0000 ± 0.0000	0.0270 ± 0.0001
Mass of solvent H ₂ O (g)	50.02 ± 0.01	25.68 ± 0.01
Mg(ClO ₄) ₂ · 6H ₂ O to adenine molar ratio	...	1.07 ± 0.01
Volume of solution used (mL)	0.390 ± 0.005	0.250 ± 0.005
Average density of film (g cm ⁻³)	1.49 ± 0.01	1.82 ± 0.02 ^a
Average thickness of sample (nm)	1160 ± 160	1170 ± 260
Molar masses of molecules in film (g mol ⁻¹)	135.13	135.13 ^b 331.30 ^c
Sample surface area (cm ²)	1.72 ± 0.10	1.72 ± 0.10
Number of molecules in sample ($\times 10^{17}$)	13.3 ± 1.7	4.48 ± 0.69 ^b 4.79 ± 0.73 ^c
Angle of incidence (°)	70	70
Irradiated area (cm ²)	1.5 ± 0.3	1.5 ± 0.3
Irradiation time (s)	3600 ± 2	3600 ± 2
Applied electron current (nA)	265 ± 20	290 ± 20
Number of electrons generated ($\times 10^{16}$)	1.79 ± 0.14	1.95 ± 0.13
Initial energy of the electrons (keV)	5.00	5.00
Average backscattered energy of the electrons (keV)	3.32 ± 0.07	3.38 ± 0.06
Average transmitted energy of the electrons (keV)	0.00 ± 0.00	0.00 ± 0.00
Fraction of backscattered electrons (%)	35.6 ± 2.5	37.5 ± 2.4
Fraction of transmitted electrons (%)	0.0 ± 0.0	0.0 ± 0.0
Simulated average penetration depth (nm)	200 ± 15	180 ± 10
Number of exposed molecules ($\times 10^{16}$)	20.1 ± 0.4	6.05 ± 1.27 ^b 6.47 ± 1.36 ^c
Dose per molecule (eV)	340 ± 77	335 ± 75 ^b 820 ± 180 ^c

Notes.

^a To calculate the average value, the density of Mg(ClO₄)₂ · 6H₂O was approximated to be 1.98 ± 0.03 g cm⁻³ (Lewis 2007).

^b Adenine.

^c Mg(ClO₄)₂ · 6H₂O.

^d Average value calculated by weighting the molar masses of adenine and Mg(ClO₄)₂ · 6H₂O with their experimentally determined molar ratios.

(Nowak et al. 1996; Mohamed et al. 2009; Evans et al. 2011). A broad and intense band can be observed in the 3450–2890 cm⁻¹ region of the neat adenine (C₅H₅N₅) sample; this originates primarily from the N–H and C–H stretching vibrations of the adenine molecule. Namely, the following vibrational modes account for this absorption feature: the very weak antisymmetric and a doublet of the symmetric stretching vibrations of the amine (–NH₂) group (ν_{as} NH₂ at 3426 cm⁻¹ and ν_s NH₂ at 3294 and 3260 cm⁻¹) as well as the stretching vibrations of the N–H and C–H moieties (ν N(9)–H at 3354 cm⁻¹, ν C(8)–H between 3190 and 3000 cm⁻¹, and ν C(2)–H) in the range of 2995–2890 cm⁻¹), respectively. The numbers in parentheses mark the label of the respective atom before them; see also Figure 1(a) for the atomic labeling of the most stable N(9)–H tautomer of the adenine (C₅H₅N₅) molecule. Similarly to the glycine (H₂NCH₂COOH) molecule—although to a lesser extent—a broad band of combinational bands and overtones can also be seen between 2885 and 2435 cm⁻¹; the broadening of all the vibrational modes mentioned above is likely caused by the Fermi resonance between the N–H and C–H stretching vibrations and these combinational bands (Góbi et al. 2016a). In the mid-IR region, the bending mode of the –NH₂ group (β NH₂, 1690 cm⁻¹) and the stretching modes of the C–N and C–C bonds of the six-membered ring of the molecule (ν CN (R6) and ν CC (R6) at 1619 and 1600 cm⁻¹ respectively) can be identified; both peaks are exceptionally strong. Note that (R5) and (R6) denote whether

the respective vibrational mode occurs in the five- or six-membered ring of the adenine molecule. Further, ring vibration modes with lower intensities can also be detected at lower wavelengths: the C–N stretching vibrations of the five- and six-membered rings (ν CN (R5) at 1509, 1338, 1257, 1235, 1165, and 1131 cm⁻¹ and ν CN (R6) at 1485 and 1315 cm⁻¹), the C–C vibration of the six-membered ring (ν CC (R6), 1459 cm⁻¹), and the C(6)–N(10) stretching vibration (ν C(6)N(10), 1374 cm⁻¹). It is worth noting that all these modes are coupled: their Potential Energy Distributions (PEDs) show that numerous vibrational modes may contribute to these vibrations and even the most significant one can have a contribution less than 20% (Table 3; for the complete PEDs, see the work of Mohamed et al. 2009). The bending mode of the C–H moieties can be found at 1424 (β C(2)H) and 1280 cm⁻¹ (β C(8)H), whereas the same mode for the N–H group (β N(9)H) is at 1066 cm⁻¹. At wavelengths of 918 and 892 cm⁻¹, vibrations of the N–C–N blocks of the five-(β NCN (R5)) and six-membered rings (β NCN (R6)) of the adenine (C₅H₅N₅) molecule can also be detected. Other peaks in the low-frequency region belong to the rocking vibration of the –NH₂ group (ρ NH₂, 1029 cm⁻¹), wagging of C–H moieties (ω C(2)H at 946 cm⁻¹ and ω C(8)H at 852 cm⁻¹), and the torsional and breathing motions of the six-membered ring (τ R6 and R6 breath at 799 and 727 cm⁻¹, respectively).

Changes were induced in the IR spectrum of the neat adenine (C₅H₅N₅) sample when irradiated with energetic electrons. The

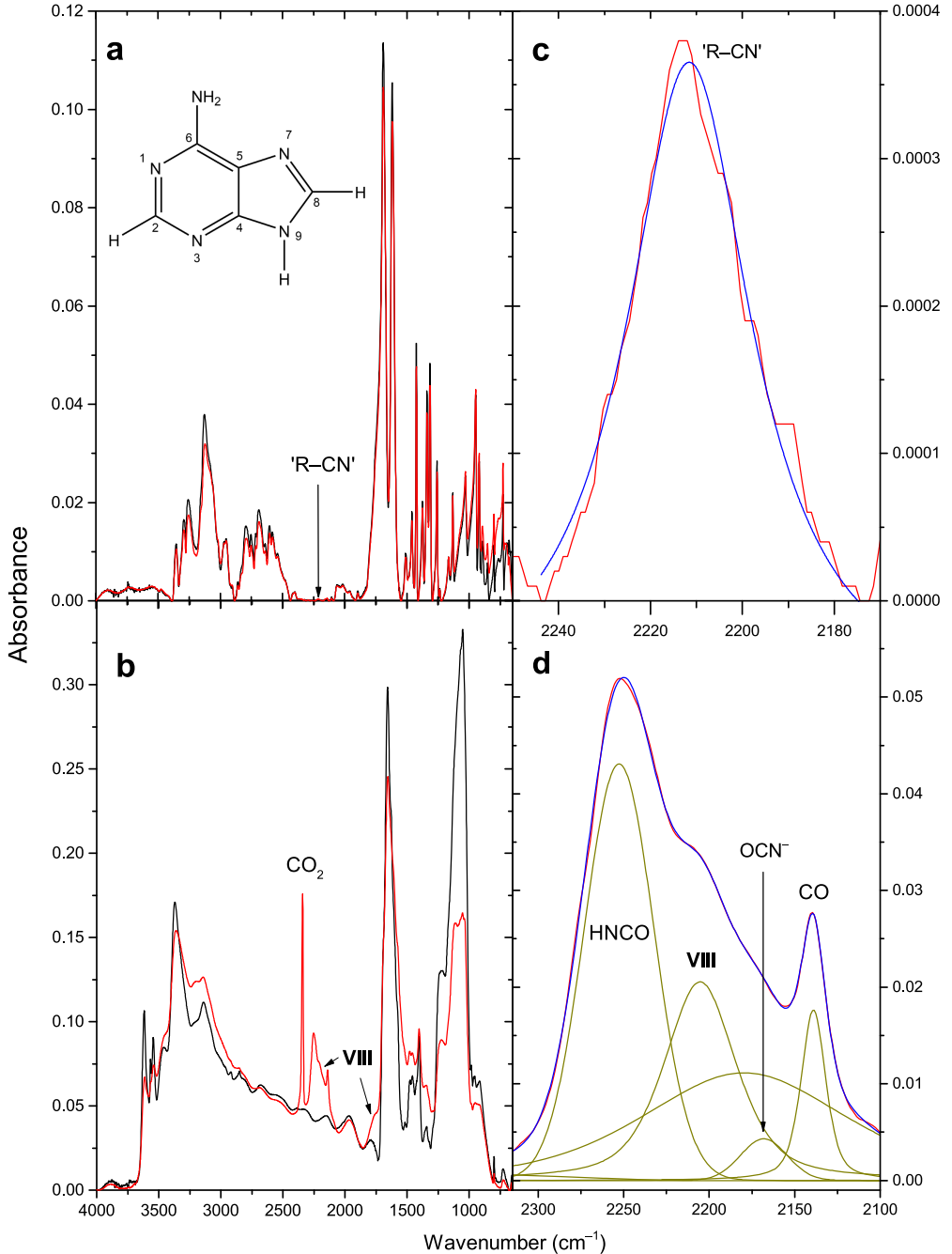


Figure 1. Infrared spectra of the (a) neat adenine and (b) adenine–Mg(ClO₄)₂ · 6H₂O 1:1 mixture prior to (black line) and after irradiation (red line). Panels (c) and (d) display selected areas of (a) and (b) showing the deconvoluted absorption peaks of the irradiation products with the following band positions: (c) 2213 cm⁻¹ (“R-CN”), (d) 2252 cm⁻¹ (HNCO), 2205 cm⁻¹ (VIII), 2168 cm⁻¹ (OCN⁻), and 2139 cm⁻¹ (CO). The inset in Figure 1(a) shows the N(9)–H tautomer of the adenine with the atomic labels.

spectra before and after the irradiation evidently differ from each other (Figure 1(a)); this is in complete accordance with radiolysis studies of adenine samples done previously (Table 1). In general, all bands decrease—and some even broaden and/or shift toward lower/higher frequencies—suggesting that the adenine (C₅H₅N₅) molecules are being efficiently destroyed during the irradiation. The broadening may be an evidence for the formation of radiolysis products as well as the degradation of the crystal structure of adenine (amorphization). Besides this ubiquitous phenomenon, there is only one new and extremely weak signal that can be observed at 2213 cm⁻¹ belonging to the

stretching vibration of the nitrile moiety (ν C≡N; Figures 1(a) and (c)) of an organic nitrile with a general formula of R-C≡N. The appearance of this functional group was predicted based on the previous electron irradiation study of adenine (C₅H₅N₅; Evans et al. 2011).

3.1.2. Adenine–Magnesium Perchlorate Hexahydrate Samples

The FTIR spectrum of the adenine (C₅H₅N₅)–magnesium perchlorate hexahydrate (Mg(ClO₄)₂ · 6H₂O) 1:1 sample is displayed in Figure 1(b), whereas the assignment of its vibrational modes is summarized in Table 3. Fundamental

Table 3Infrared Absorption Peak Assignments for the Neat Adenine and the Adenine–Mg(ClO₄)₂ · 6H₂O 1:1 Samples as well as for the Irradiation Products Before and After the Electron Radiolysis

Mohamed et al. (2009) ^a	Evans et al. (2011) ^a	Adenine			Adenine–Mg(ClO ₄) ₂ · 6H ₂ O 1:1			Mode ^{c,d}	Assignment ^{c,d}
		Pre-irrad ^b	Post-irrad ^b	Change Upon Irrad. ^b	Pre-irrad ^b	Post-irrad ^b	Change Upon Irrad. ^b		
...	N/A	3617s	3614 m,b	-, b	$\nu_3(\text{H}_2\text{O})^e$	$\nu_{\text{as}} \text{OH}$
...	N/A	3567 m, 3546 m	3567sh, 3540w, b	-, b	$\nu_1(\text{H}_2\text{O})^e$	$\nu_{\text{s}} \text{OH}$
3426vw	3426vw	3426vw	3458 m	3450sh	-, b	ν_3	$\nu_{\text{as}} \text{NH}_2$ (100)
3347sh	3354 m	3354 m	3354 m	...	3369s	3360s	-, b	ν_2	$\nu \text{N(9)H}$ (100)
3296	3294 m, 3260 m	3294 m, 3260 m	3294 m, 3256 m	...	3293sh	3293sh	-, b	ν_1	$\nu_{\text{s}} \text{NH}_2$ (100)
3119vs	3154sh, 3131s, 3087sh, 3063sh, 3023sh	3131s, 3087sh, 3063sh, 3020sh	3123s, 3087sh, 3063sh,	-, b	3193sh, 3142 m	3192sh, 3145w	-, b	ν_4	$\nu \text{C(8)H}$ (99)
2980s	2969 m, 2954 m, 2922sh	2969 m, 2952 m	2952 m	-, b	2957sh, 2918w	2921sh	...	ν_5	$\nu \text{C(2)H}$ (100)
...	2885–2435	2885–2435	2885–2435	N/A	N/A	combinational bands, overtones
...	N/A	...	2342s	+	$\nu_3(\text{CO}_2)$	$\nu_{\text{as}} \text{CO}_2$
...	N/A	...	2276sh, 2252 m	+	$\nu_2(\text{HNCO})$	$\nu_{\text{as}} \text{N}=\text{C}=\text{O}$
...	2235w	...	2213w	+	N/A	$\nu(\text{R}-\text{C}\equiv\text{N})$	$\nu \text{C}\equiv\text{N}$
7									I, II, III, IV?
...	2235w	N/A	...	2205sh	+	$\nu(\text{C}_4\text{H}_4\text{N}_4\text{O, VIII})$	$\nu \text{C}\equiv\text{N}$
...	N/A	...	2168sh	+	$\nu_3(\text{OCN}^-)$	$\nu_{\text{as}} \text{OCN}^-$
...	N/A	...	2139w	+	$\nu_1(\text{CO})$	νCO
...	N/A	...	1870vw	+	$\nu_1(\text{NO})$	νNO
...	N/A	...	1749sh	+	$\nu(\text{C}_4\text{H}_4\text{N}_4\text{O, VIII})^g$	$\nu \text{C}=\text{O}$
1673vs	1681	1690vs	1689vs	-, b	1658vs, 1628sh, 1578sh	1655vs, 1613sh, 1578sh	-, b	ν_6	βNH_2 (54)
...	N/A				$\nu_2(\text{H}_2\text{O})^e$	βOH
1603vs	1609	1619vs	1616vs	-, b				ν_7	$\nu \text{CN(R6)}$ (29)
1603vs	...	1600sh	1600sh	-, b				ν_8	$\nu \text{CC(R6)}$ (31)
1506sh	1506 ^h	1509 m,b	1509 m,b	...	1516w	1521sh	-, b	ν_9	$\nu \text{CN(R5)}$ (32)
1483sh	...	1485sh	1485sh	...	1475 m	1481w	...	ν_{10}	$\nu \text{CN(R6)}$ (24)
1451 m	1456	1459 m	1459 m	...	1457 m	1457w	...	ν_{11}	$\nu \text{CC(R6)}$ (19)
1420s	1420	1424s	1424s	...	1404 m	1401 m	...	ν_{12}	$\beta \text{C(2)H}$ (37)
1368w	1368 ^h	1374 m	1373 m	...	1357sh	1354sh	...	ν_{13}	$\nu \text{C(6)N(10)}$ (13)
1335s	1335 ^h	1338s	1338s	...	1342w	1345w	...	ν_{14}	$\nu \text{CN(R5)}$ (20)
1309s	1309 ^h	1315s	1314s	...	1319sh	1319sh	...	ν_{15}	$\nu \text{CN(R6)}$ (48)
...	N/A	1289sh	1289vw	...	$2\nu_4(\text{ClO}_4^-)$	$2\beta_{\text{as}} \text{ClO}_4^-$
1252s	...	1280sh	1280sh	...	1221s, 1165sh, 1119sh, 1091sh, 1068sh, 1052vs	1224s, 1167sh, 1111s, 1068sh, 1053s, 1037sh	...	ν_{16}	$\beta \text{C(8)H}$ (26)
1252s	1255 ^h	1257s, 1235w	1257 m, 1235w	...				ν_{17}	$\nu \text{CN(R5)}$ (19)
1126	1160 ^h , 1126	1165w, 1131 m	1164w, 1130 m	...				ν_{18}	$\nu \text{CN(R5)}$ (18)
...	N/A				$\nu_3(\text{ClO}_4^-)$	$\nu_{\text{as}} \text{ClO}_4^-$
1065sh	...	1066sh	1066sh	...				ν_{19}	$\beta \text{N(9)H}$ (35)
1025 m	1021	1029 m	1028 m	...				ν_{20}	ρNH_2 (41)
...	N/A	983w, 962w, 954w	983vw, 954sh	...	$\nu_1(\text{ClO}_4^-)$	$\nu_{\text{s}} \text{ClO}_4^-$

Table 3
(Continued)

Mohamed et al. (2009) ^a	Evans et al. (2011) ^a	Adenine			Adenine–Mg(ClO ₄) ₂ · 6H ₂ O 1:1			Mode ^{c,d}	Assignment ^{c,d}
		Pre-irrad ^a	Post-irrad ^a	Change Upon Irrad. ^b	Pre-irrad ^a	Post-irrad ^a	Change Upon Irrad. ^b		
939s	944 ^h	946s	946s	...	949sh	949vw, b	...	ν_{21}	ω C(2)H (100)
913s	914 ^h	918 m	918 m	...	916w, b	916sh	...	ν_{22}	β NCN(R5) (54)
872sh	...	892w	893w	–, b	871sh	871sh	...	ν_{23}	β NCN(R6) (51)
846sh	850	852w	851w	–, b				ν_{24}	ω C(8)H (100)
797w	800	799w	799w	...	797w	797w	...	ν_{25}	τ R6 (81)
723 m	723	727 m	727 m	...	727w, b	724w, b	...	ν_{26}	R6 breath (22)

Notes.

^a Wavenumber in cm⁻¹, vs: very strong, s: strong, m: medium, w: weak, vw: very weak, sh: shoulder, b: broad, –: no signal.

^b –/+: decrease/increase of signal, b: broadening upon irradiation, N/A: not applicable.

^c Assignment of the adenine vibrations based on Mohamed et al. (2009), level of theory used: MP2/6-31G(d). Only the vibrational modes with the biggest PED contributions (in parentheses after the vibrational mode, given in percentage) are listed; see full PED in reference. Type of vibrational modes: ν : stretching, β : bending (scissoring), ρ : rocking, ω : wagging, τ : torsional, s: symmetric, as: antisymmetric; $2\beta_{as}$ ClO₄[–] denotes the first overtone of the antisymmetric bending vibration of the ClO₄[–] unit. The number in parentheses after the atom shows its label; see the inset in Figure 1(a) for the atomic labeling of the adenine molecule. (R5): five-membered ring, (R6): six-membered ring. N/A: not applicable, ?: tentative assignment.

^d Assignment of other species are based on the following references: Miller & Wilkins (1952), Bishop et al. (2014), and Hanley et al. (2015) for Mg(ClO₄)₂ · 6H₂O; Gerakines et al. (1995) for CO and CO₂; Fateley et al. (1959) and Stirling et al. (1994) for NO; Broekhuizen et al. (2004) and Bennett et al. (2010) for OCN[–]; Lowenthal et al. (2002), and Broekhuizen et al. (2004) for HNCO; Seki & Ikariya (2009) for VIII.

^e Vibrations of crystalline water in Mg(ClO₄)₂ · 6H₂O.

^f Formed in the irradiated neat adenine sample.

^g Formed in the irradiated adenine–Mg(ClO₄)₂ · 6H₂O 1:1 mixture sample.

^h Reassigned modes.

differences are observed when comparing the FTIR spectra of the neat and mixture samples. Most importantly, the characteristic broad band of the combinational bands and overtones of the vibrational modes of neat adenine ($C_5H_5N_5$) between 2885 and 2435 cm^{-1} disappears in the mixture sample; furthermore, most of the peaks are shifted toward lower or higher wavelengths, and several new absorption peaks can be detected. One of these new signals can be assigned to the antisymmetric ($\nu_{as}\text{ OH}$, 3617 cm^{-1}) and symmetric ($\nu_s\text{ OH}$, 3567 and 3546 cm^{-1}) stretching vibrations of the O–H functional group of the crystalline water in magnesium perchlorate hexahydrate ($Mg(ClO_4)_2 \cdot 6H_2O$). The other, more prominent new absorption feature belongs to the antisymmetric ($\nu_{as}\text{ ClO}_4^-$, in the region of 1310 – 990 cm^{-1}) and symmetric vibrations ($\nu_{as}\text{ ClO}_4^-$, between 990 and 940 cm^{-1}) of the perchlorate unit (Miller & Wilkins 1952; Bishop et al. 2014; Hanley et al. 2015). A weak shoulder is also detectable at 1289 cm^{-1} caused by the second harmonic of the antisymmetric bending vibration of the perchlorate unit ($2\beta_{as}\text{ ClO}_4^-$). The position and shape of the perchlorate vibrational band also agrees well with our previous results (Góbi et al. 2016a, 2016b, 2017). It is worth noting that multiple vibrational modes of the adenine ($C_5H_5N_5$) molecule overlap with this particularly intense band of the perchlorate unit (ClO_4^-); these are the stretching vibrations of the C–N molecules in the five-membered ring ($\nu\text{ CN (R5)}$), the bending motions of C–H ($\beta\text{ C(8)H}$) and N–H ($\beta\text{ N(9)H}$) moieties, the rocking of the –NH₂ group ($\rho\text{ NH}_2$), and the wagging of a C–H bond ($\omega\text{ C(2)H}$). The best example for the aforementioned change in band positions is the stretching vibration of the –NH₂ functional group; its maximum moves by $+32\text{ cm}^{-1}$ to 3458 cm^{-1} in the mixture sample. This phenomenon—similarly to the case of glycine (H_2NCH_2COOH , (Góbi et al. 2016a))—might be explained by the possible formation of hydrogen bonds with the oxygen atoms of crystalline water in magnesium perchlorate hexahydrate ($Mg(ClO_4)_2 \cdot 6H_2O$), although to a smaller extent, almost all modes are shifted at least by ± 10 – 20 cm^{-1} compared to the neat adenine ($C_5H_5N_5$) samples. The bending vibration of crystalline water ($\beta\text{ OH}$) can be detected at around 1624 cm^{-1} , which is also superposed by some of the adenine ($C_5H_5N_5$) vibrational modes, namely the –NH₂ bending ($\beta\text{ NH}_2$) and C–N and C–C vibrations of the six-membered ring ($\nu\text{ CC (R6)}$ and $\nu\text{ CN (R6)}$), causing them to merge into one absorption peak with exceptionally high intensity. The last apparent difference between the neat sample and the mixture with magnesium perchlorate hexahydrate ($Mg(ClO_4)_2 \cdot 6H_2O$) is the merger of two peaks resulting in a shoulder of the broad perchlorate absorption feature: the bending motion of the NCN atoms in the six-membered ring ($\beta\text{ NCN (R6)}$) and the wagging of one of the C–H group ($\omega\text{ C(8)H}$).

Similar conclusions can be drawn if the sample containing both adenine ($C_5H_5N_5$) and magnesium perchlorate hexahydrate ($Mg(ClO_4)_2 \cdot 6H_2O$) is irradiated with high-energy electrons: besides the ubiquitous decrease of the fundamentals, broadening, and shift of the reactant peaks—due to the degradation and amorphization of the crystal structure—the formation of new species can also be observed. However, in contrast to the neat samples, this phenomenon is more emphasized; numerous new and intense carriers emerge upon irradiation particularly in the region of 2400 – 2050 cm^{-1} (Figure 1b). The broadening is especially prominent in the case of the –NH₂ ($\nu_{as}\text{ NH}_2$, peak maximum at 3450 cm^{-1} after

irradiation), N–H ($\nu\text{ N(9)H}$, 3360 cm^{-1}), and C–H ($\nu\text{ C(8)H}$ and $\nu\text{ C(2)H}$, at 3145 and 2921 cm^{-1} , respectively) stretching vibrations at wavelengths between 3500 and 2900 cm^{-1} . The same holds true for the region of 1850 – 1310 cm^{-1} comprising two new emerging signals, and the already well-known absorptions of the stretching modes of the C–N ($\nu\text{ CN (R5)}$ at 1521 and 1345 cm^{-1} after irradiation, $\nu\text{ CN (R6)}$ at 1481 and 1319 cm^{-1}) and C–C vibrations of the five- and six-membered rings, the bending motions of the –NH₂ ($\beta\text{ NH}_2$) and O–H moieties ($\beta\text{ OH}$, both of them at around 1655 cm^{-1} along with other C–C and C–N vibrations), and that of one C–H group ($\beta\text{ C(2)H}$ at 1401 cm^{-1}).

The aforementioned new absorption signals can be found at 2342 cm^{-1} , between 2310 and 2060 cm^{-1} , and as a shoulder in the range of 1850 – 1730 cm^{-1} . The first one can be assigned as the antisymmetric stretching vibration of the carbon dioxide (CO_2) molecule (Gerakines et al. 1995), whereas the last one belongs to a carbonyl stretching vibration ($\nu\text{ C=O}$) of a hitherto unknown adenine ($C_5H_5N_5$) irradiation product (denoted as species VIII thereafter, Table 3; see also Section 4.1.2) and possibly to the stretching vibration of the nitrogen monoxide (NO) molecule ($\nu\text{ NO}$, 1870 cm^{-1} (Fateley et al. 1959; Stirling et al. 1994)). The second feature consists of multiple peaks that can be deconvoluted as seen in Figure 1(d); the maxima of these peaks are at 2252 , 2205 , 2168 , and 2139 cm^{-1} . These can be assigned to the $N=C=O$ antisymmetric vibration of the HNCO (isocyanic acid, Lowenthal et al. 2002; Broekhuizen et al. 2004) molecule ($\nu_{as}\text{ NCO}$), the stretching vibration of the $C\equiv N$ ($\nu\text{ CN}$) in an organic nitrile molecule ($R-C\equiv N$, similarly to the neat adenine sample although it is likely caused by species VIII, the antisymmetric stretching vibration of the OCN^- (isocyanate) ion ($\nu_{as}\text{ OCN}^-$, Broekhuizen et al. 2004; Bennett et al. 2010)), and the stretching vibration of the CO (carbon monoxide) molecule (Gerakines et al. 1995). The formation of new irradiation products agrees well with the findings of Evans et al. (2011); they also identified the $R-C\equiv N$ and $R-C=O$ groups as well as the presence of nitrogen monoxide (NO) at 1870 cm^{-1} , although the latter was assigned to the stretching vibration of the carbonyl group as well. It is also likely that the general broadening of the adenine ($C_5H_5N_5$) peaks upon irradiation is at least partially caused by the formation of other new radiolysis products, similarly to the case of irradiated glycine (H_2NCH_2COOH)—magnesium perchlorate hexahydrate ($Mg(ClO_4)_2 \cdot 6H_2O$, (Góbi et al. 2016a, 2017)), where ammonia (NH_3) and methylamine (CH_3NH_2) were both observed.

3.2. TPD Profiles of Adenine and Adenine–Magnesium Perchlorate Hexahydrate Samples

3.2.1. Species Related to the Electron Radiolysis of the Adenine–Nitrogen Monoxide, Cyanamide, and Cyanoimidogen Radical

Figure 2(a) shows the EI-QMS TPDs of $m/z = 28$ (black), 32 (red), and 44 (blue), whereas Figures 2(b)–(f) reveal the PI-ReTOF-MS TPDs of $m/z = 30$ (Figure 2(e)), 40 (Figure 2(c)), 42 (Figure 2(d)), 67 , 69 (Figure 2(b)), and 135 (Figure 2(f)). The species with the lowest mass-to-charge ratio in the PI-ReTOF-MS spectrum (30) is nitrogen monoxide (NO, Figure 2(e), ionization energy (IE) = 9.2643 ± 0.0002 , (Ebata et al. 1983)), which starts subliming at 250 K and appears only in the sample containing oxygen atoms upon irradiation (adenine ($C_5H_5N_5$)—magnesium perchlorate hexahydrate ($Mg(ClO_4)_2 \cdot 6H_2O$) 1 : 1 mixture); its presence is also confirmed

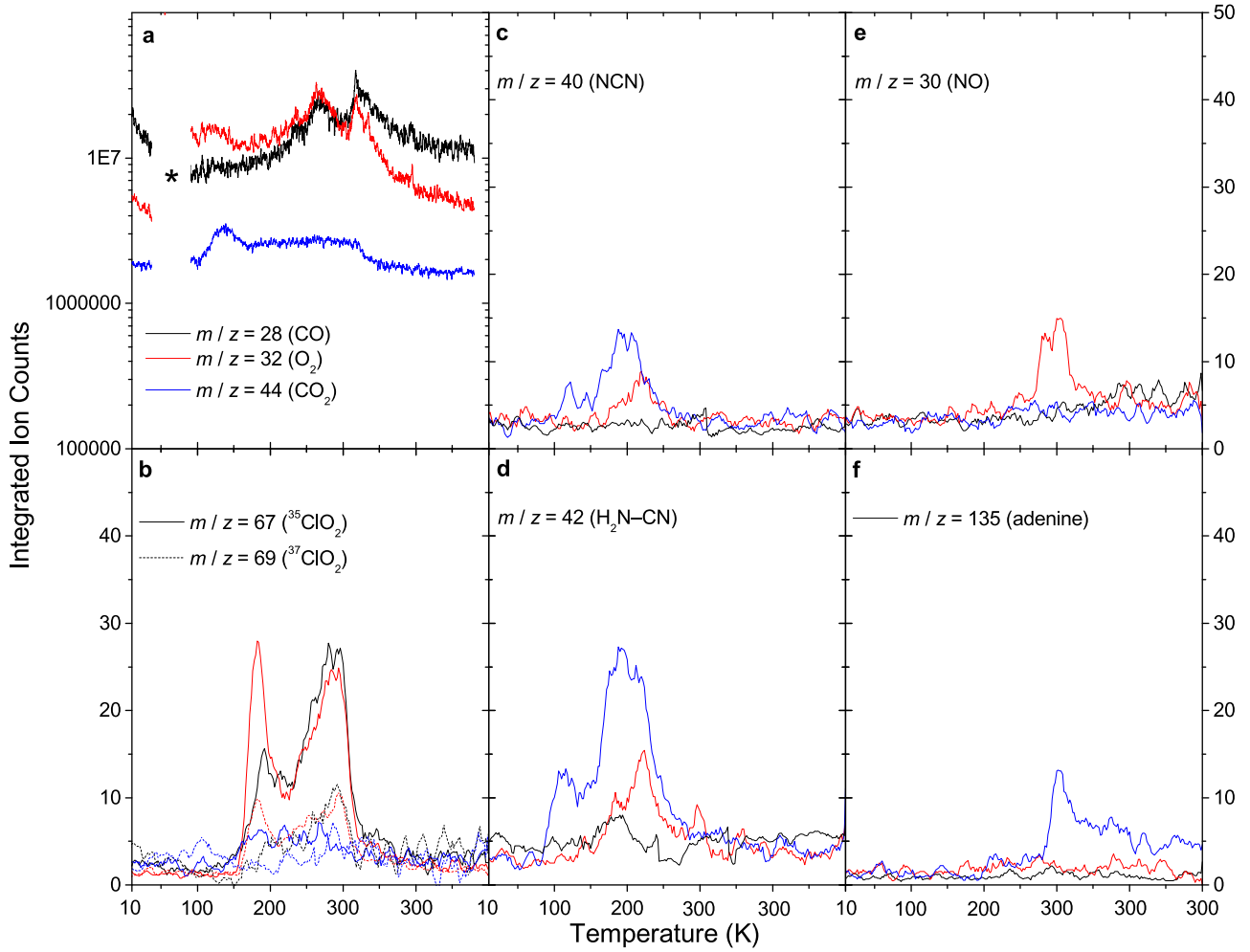


Figure 2. EI-QMS of the neat adenine sample (a) and PI-ReTOF-MS (b)–(f) TPD profiles of neat $Mg(ClO_4)_2 \cdot 6H_2O$ (black line, the data presented in Góbi et al. 2016b), neat adenine (blue) and the adenine– $Mg(ClO_4)_2 \cdot 6H_2O$ 1:1 mixture (red) samples. The panels show the species with the following m/z values: (a) 28 (CO, black), 32 (O_2 , red), and 44 (CO_2 blue), (b) 67 ($^{35}ClO_2$, solid line) and 69 ($^{37}ClO_2$, dashed line), (c) 40 (NCN), (d) 42 (H_2N-CN), (e) 30 (NO), and (f) 135 (adenine). The asterisk in panel (a) shows a masked artifact caused by the saturation of the detector due to the extremely intense O_2 peak signal.

by its IR signal (see Section 3.1.2 and Table 3). This is in contrast to the value obtained by previous PI-ReTOF-MS TPD investigations that successfully produced nitrogen monoxide in situ by electron radiolysis of solid nitromethane (CH_3NO_2) ices (Kaiser & Maksyutenko 2015; Maksyutenko et al. 2016). They found that the irradiation product nitrogen monoxide starts subliming at around 150 K and the elevated sublimation temperature in the current study implies that this species forms by the oxidation of adenine ($C_5H_5N_5$) or its irradiation product(s) and is presumably associated with the heating of the sample (Section 4.1.2).

In contrast to nitrogen monoxide (NO), the signal of the parent molecular ion of the adenine ($C_5H_5N_5$, IE = 8.2 ± 0.03 , (Schwell et al. 2006)) at $m/z = 135$ can only be detected in neat adenine and completely disappears in the mixture sample due to the oxidation reactions as detailed below; its sublimation starts at approximately 280 K (Figure 2(f)). It is worth noting that adenine does not undergo dissociative photoionization below IEs of 12 eV (Pilling et al. 2007), thus none of its fragments is expected to show up in the PI-ReTOF-MS TPD profiles. There are two signals that can be attributed to the radiolytic destruction of adenine ($C_5H_5N_5$) and can be detected at $m/z = 40$ (Figure 2(c)) and 42 (Figure 2(d)). Whereas the latter possibly belongs to cyanamide ($H_2N-C\equiv N$, IE = 10.4 eV (Guimon et al. 1989)), the former is a

likely fragmentation product of cyanamide formed by H_2 -loss (cyanoimidogen, $N-C\equiv N$), justified by their almost identical peak position and shape although its appearance and ionization energies upon photoionization are unknown. It is important to point out that this species cannot account for the FTIR signal at 2213 and 2205 cm^{-1} in the neat and mixture samples as its absorbs at higher wavelengths (2264 cm^{-1} , King & Strope 1971). The same holds true for the new IR band at 2252 cm^{-1} in the mixture sample; as the signal of cyanamide in the PI-ReTOF-MS spectrum becomes even smaller compared to that of the neat adenine ($C_5H_5N_5$) sample, it cannot account for the appearance of an intense new absorption peak in the FTIR spectrum. The lower PI-ReTOF-MS signal in the adenine–magnesium perchlorate hexahydrate ($Mg(ClO_4)_2 \cdot 6H_2O$) 1:1 mixture also implies that cyanamide may also be oxidized in the presence of an oxidizing agent; see Figures 3 and 4 and Section 4.1 for more details on its possible formation mechanisms. Their sublimation temperature also shifted toward higher temperatures that can be caused by the different molecular environment, the presence of magnesium perchlorate hexahydrate. The other irradiation products detected by means of the FTIR spectrometer have IEs too high to be ionized by the photoionization energy used; these are 14.0142 ± 0.0003 (CO, Erman et al. 1993), 11.759 ± 0.006 (OCN radical, Ruscic & Berkowitz

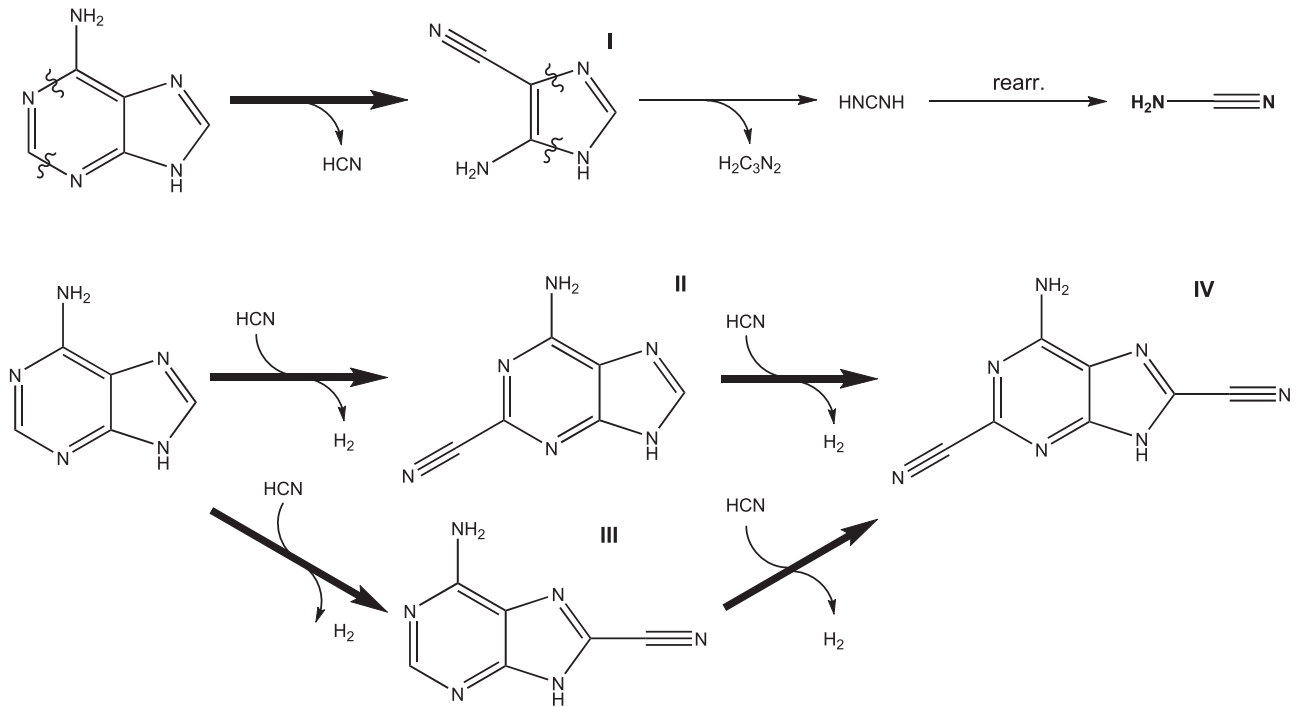


Figure 3. Proposed decomposition mechanism of adenine and formation pathway of species R-CN in the neat adenine sample upon energetic electron irradiation. The hydrogen atoms bound to carbon atoms are not shown.

1994), 11.595 ± 0.005 (HNCO, Ruscic & Berkowitz 1994), and 13.774 ± 0.003 eV (CO_2 , Parr & Taylor 1974).

3.2.2. Species Related to the Oxidation of Adenine in the Adenine–Magnesium Perchlorate Hexahydrate Samples

Carbon monoxide (CO , $m/z = 28$, black), molecular oxygen (O_2 , $m/z = 32$, red), and carbon dioxide (CO_2 , $m/z = 44$, blue) molecules are all clearly visible in the EI-QMS of the irradiated adenine ($\text{C}_5\text{H}_5\text{N}_5$)–magnesium perchlorate hexahydrate ($\text{Mg}(\text{ClO}_4)_2 \cdot 6\text{H}_2\text{O}$) 1:1 mixture (Figure 2(a)). This finding thus nicely complements the PI-ReTOF-MS measurements as the IEs of these species are higher (12.0697 ± 0.0002 eV (Tonkyn et al. 1989) for O_2 ; see Section 3.2.1 for those of the other two species) than the photoionization energy used (10.49 eV) and therefore they could not be detected via the latter method. The carbon dioxide (CO_2) signal has a similar sublimation profile to the one found in a previous experiment that used electron irradiation of carbon dioxide (CO_2)–hydrocarbon ice mixtures to produce carboxylic acids (R– COOH , Kim & Kaiser 2010); its presence is also confirmed by the FTIR spectrum of the sample (Figure 1(b)).

The molecular oxygen (O_2) has two maxima in its TPD profile, the first at around 55 K being close to the sublimation temperature of the neat oxygen ices (Bennett et al. 2014), indicating that it is caused by the subliming unreacted oxygen molecules. Although this signal could not be detected previously in irradiated samples containing perchlorates (Góbi et al. 2016a, 2016b, 2017), this can be explained by the approximately 20 times higher dose exploited here (820 versus 40 eV per magnesium perchlorate hexahydrate ($\text{Mg}(\text{ClO}_4)_2 \cdot 6\text{H}_2\text{O}$) molecule), allowing for the formation of significantly more molecular oxygen as well as the more thorough destruction of the structure of the sample, which thus cannot withhold the volatiles at higher temperatures. The second sublimation event of oxygen has a broad profile and starts at about 200 K; it has a remarkably similar shape to the one that

could be obtained by irradiating neat magnesium perchlorate hexahydrate ($\text{Mg}(\text{ClO}_4)_2 \cdot 6\text{H}_2\text{O}$) samples and can be assigned to the oxygen released during the thermal decomposition of various chlorine oxides (Cl_xO_y ; $x = 1, 2$, $y = 1–7$) formed upon the electron irradiation of the perchlorate unit (Góbi et al. 2016b). This is also in coincidence with the second maxima (at around 285 K) of the $35\text{-}^{35}\text{ClO}_2$, $m/z = 67$) and 37-chlorine dioxide ($^{37}\text{ClO}_2$, $m/z = 69$) signals in the adenine ($\text{C}_5\text{H}_5\text{N}_5$)–magnesium perchlorate hexahydrate ($\text{Mg}(\text{ClO}_4)_2 \cdot 6\text{H}_2\text{O}$) 1 : 1 mixture sample (Figure 2(b)), indicating their formation by the decomposition of the higher chlorine oxides.

The first maxima of the chlorine dioxide isotopologue signals could be obtained at about 190 K caused by these molecules formed in situ in the sample upon irradiation as found previously (Góbi et al. 2016b). This finding is also justified by the fact that this peak is proportionally more intense in the mixture samples (Figure 2(b), red) than that of the neat perchlorate (ClO_4^-) samples used in our earlier work (Figure 2(b), black). This may be due to the fact that the doses used in the current experiment was about 20 times higher, resulting in a more effective in situ formation of chlorine dioxide (ClO_2) due to the more complete destruction of the perchlorate (ClO_4^-) unit and higher chlorine oxides (Cl_xO_y , $x = 1, 2$, $y = 1–7$) upon irradiation. Alternatively, the first sublimation event might be caused by the molecules subliming from the upper, irradiated, and therefore altered (amorphized) layer, whereas the second, broader band may be accounted for by the molecules that diffused to the deeper, intact layers of the sample in the early stages of the TPD phase, which allows them to sublime at higher temperatures. It is important to point out that none of these species (O_2 , CO_2 , ClO_2) mentioned above can be found in the irradiated neat adenine ($\text{C}_5\text{H}_5\text{N}_5$) samples.

The signal of carbon monoxide could also be observed in the EI-QMS spectrum, likely predominantly from the carbon

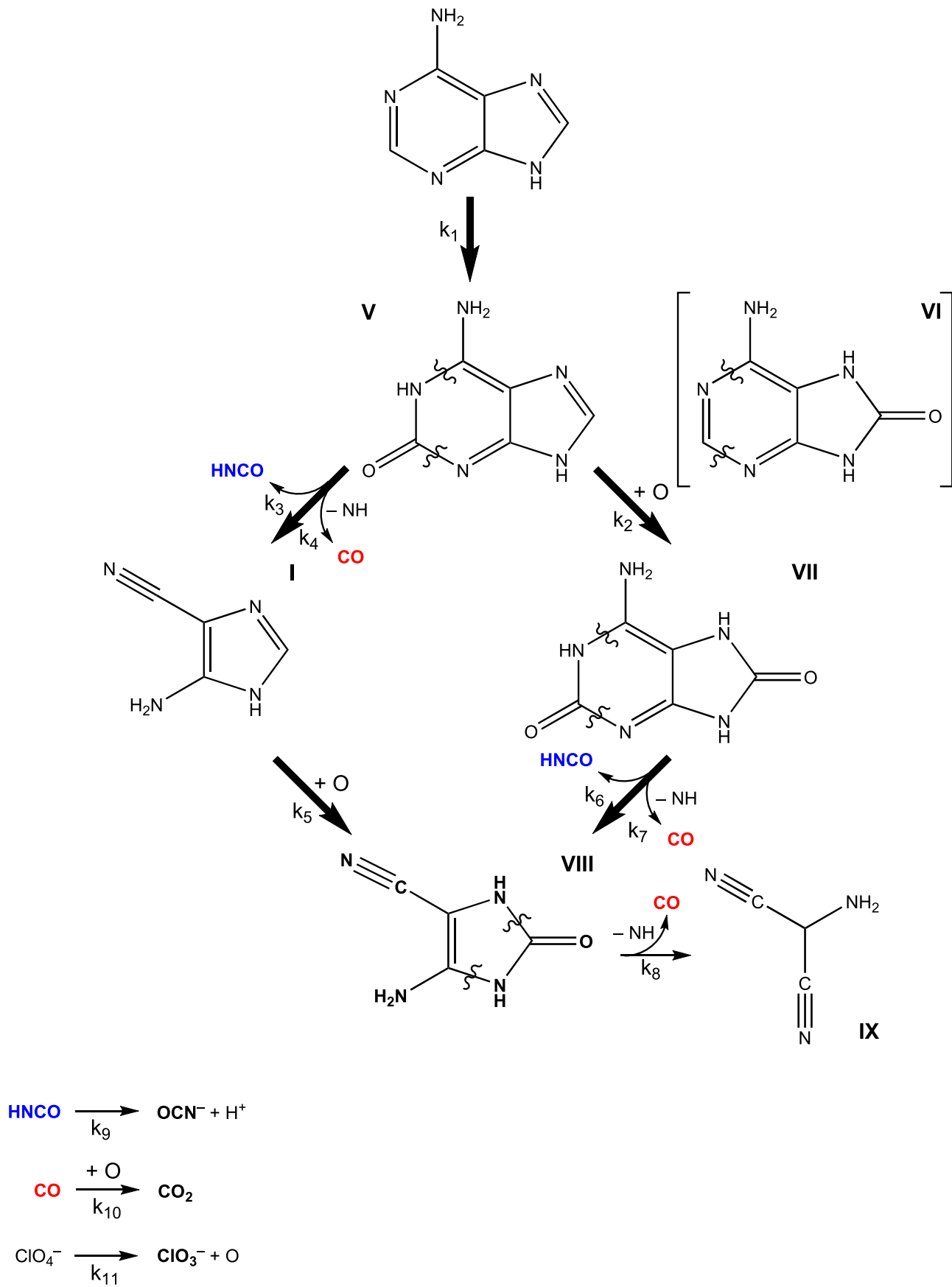


Figure 4. Proposed decomposition pathway of adenine and formation pathways of the irradiation products in the adenine–Mg(ClO₄)₂ · 6H₂O 1:1 mixture sample upon energetic electron irradiation. Species VI in parentheses shows the unobserved derivative of molecule V. The hydrogen atoms bound to carbon atoms are not shown.

Table 4

Irradiation Products Detected in the Neat Adenine and the Adenine–Mg(ClO_4)₂ · 6H₂O 1:1 Samples via the FTIR, PI-ReTOF-MS, and EI-QMS Techniques

Method	Adenine	Adenine–Mg(ClO_4) ₂ · 6H ₂ O 1:1
FTIR	R–C≡N	CO NO OCN [−] HNCO CO ₂ C ₄ H ₄ N ₄ O (VIII)
PI-ReTOF-MS	N–C≡N H ₂ N–C≡N	NO N–C≡N H ₂ N–C≡N ³⁵ ClO ₂ ³⁷ ClO ₂
EI-QMS	...	CO O ₂ CO ₂

monoxide (CO) directly with smaller contributions from the fragmentation upon 70 eV electron ionization of isocyanic acid (HNCO), and other species formed upon irradiation. In summary, a plethora of different radiolysis products can be observed in both samples as summarized in Table 4. These show that the vibrational modes of an organic nitrile group (R–C≡N) and the presence of cyanamide (H₂N–C≡N) and its photofragment cyanoimidogen radical (N–C≡N) in the PI-ReTOF-MS spectrum can be detected in the neat adenine (C₅H₅N₅) samples upon irradiation. The formation of oxidized products can be seen in the FTIR spectrum of the irradiated adenine–magnesium perchlorate hexahydrate (Mg(ClO_4)₂ · 6H₂O) mixture sample besides cyanamide and the cyanoimidogen radical such as carbon dioxide (CO₂), nitrogen monoxide (NO), isocyanate anion (OCN[−]), isocyanic acid (HNCO), carbon monoxide (CO), and chlorine dioxide (ClO₂) isotopes, and species VIII with a thus-far unknown structure discussed in Section 4.1.2 in detail. Some of these can also be detected with different methods, for instance the nitrogen monoxide (NO) via PI-ReTOF-MS and carbon dioxide (CO₂) with the help of EI-QMS. The molecular oxygen (O₂) forming upon the radiolysis of the magnesium perchlorate hexahydrate (Mg(ClO_4)₂ · 6H₂O) can also be monitored by the EI-QMS device as has been previously shown in earlier radiolysis studies as well (Góbi et al. 2016b; Turner et al. 2016).

4. Discussion

4.1. Decay Mechanisms of Adenine

4.1.1. Neat Adenine Samples

The proposed decomposition mechanism of the irradiated neat adenine (C₅H₅N₅) is shown in Figure 3. According to earlier decomposition studies (Rice & Dudek 1967; Schwell et al. 2006; Chen et al. 2011; Minaev et al. 2014), the first step of the adenine molecule decomposition is the cleavage of the N(1)–C(6) and C(2)–N(3) bonds resulting in the loss of a hydrogen cyanide (HCN) molecule. This latter species may then take part in a nucleophile substitution on carbon atoms C(2) and/or C(8) of another intact adenine molecule yielding 2-cyano adenine (II, C₆H₄N₆) and 8-cyano adenine (III, C₆H₄N₆) or might even lead to the eventual formation of 2, 8-dicyano adenine (IV, C₇H₃N₇, Evans et al. 2011). It is important to note that II and III are detected precursors in prebiotic adenine formation (Voet &

Schwartz 1983; Miller & Cleaves 2007). The other irradiation product of the hydrogen cyanide loss is 1H-5-aminoimidazol-4-carbonitrile (I, C₄H₄N₄, formally the tetramer of HCN), which can further lose a carbodiimide (HNCNH) after the breakage of the N(1)–C(5) and N(3)–C(4) bonds to form the radical H₂C₃N₂ (Rice & Dudek 1967; Schwell et al. 2006; Chen et al. 2011; Minaev et al. 2014). The carbodiimide can quickly rearrange into its more stable tautomer cyanamide (H₂N–C≡N, Maier et al. 1996) and can be detected via the PI-ReTOF-MS method. It is straightforward to assume that I, II, and III, (and presumably IV) may all account for the R–C≡N absorption peak at 2213 cm^{−1} in the FTIR spectrum of the irradiated neat adenine (C₅H₅N₅) sample.

4.1.2. Adenine–Magnesium Perchlorate Hexahydrate Samples

According to the FTIR, EI-QMS, and PI-ReTOF-MS results, a completely different radiolysis mechanism becomes predominant in the presence of an oxidizing agent as revealed in Figure 4. In the first step, the adenine (C₅H₅N₅) molecule reacts with an active oxygen atom (O) originating from the radiolysis of magnesium perchlorate hexahydrate (Mg(ClO_4)₂ · 6H₂O). The oxygen atom attacks the C(2) atom of adenine, yielding 2-oxo adenine (or isoguanine, V, C₅H₅N₅O); this product is expected to be the preferred over the alternative oxidation product 8-oxo adenine (VI, C₅H₅N₅O), which could not be detected in oxidized samples (Ibañez et al. 2015). Furthermore, the decomposition products of VI cannot be observed, contrary to those of species V, and its omission from the decomposition scheme was also confirmed by kinetic studies (Section 4.3.2).

Molecule V then can either be oxidized further into the dioxo-derivative (2,8-dioxo adenine, VII, C₅H₅N₅O₂, (Ibañez et al. 2015)) or lose an isocyanic acid (HNCO) and/or carbon monoxide (CO) molecule, resulting in the formation of I, which is also an irradiation product molecule during the neat adenine (C₅H₅N₅) radiolysis as discussed in Section 4.1.1. It should be pointed out that the isocyanic acid (HNCO) or carbon monoxide (CO) loss by the cleavage of bonds N(1)–C(6) and C(2)–N(3) in molecule V during irradiation is very similar to the first degradation step in the irradiated neat adenine sample. After this, VII can be oxidized to yield 1H-5-aminoimidazol-2-oxo-4-carbonitrile (VIII, C₄H₄N₄O). The evidence for the presence of VIII in the sample is the new arising shoulder in the FTIR spectrum of the mixture sample at roughly 1750 cm^{−1} assigned to carbonyl stretching vibration (ν C=O). It is imperative to note that the carbonyl stretching bands generally lie at lower wavelengths (below 1700 cm^{−1}); a vibrational frequency this high implies a constrained cyclic structure such as the five-membered ring in a 2-imidazolidinone-like (C₃H₆N₂O) molecule. In an earlier work, Seki & Ikariya (2009) obtained a similar carbonyl vibrational absorption feature when they successfully synthesized 1,3-dimethyl-2-imidazolidinone (C₅H₁₂N₂O) on activated silica surfaces. Alternatively, VII could also account for this absorption peak having a similar ring structure as VIII; however, it is straightforward to assume that it can take part in similar degradation reactions like the adenine (C₅H₅N₅) molecule and V along with the loss of isocyanate (HNCO) and carbon monoxide (CO) verified by the kinetic study (Section 4.3.2). Eventually, VIII can also lose an isocyanic acid (HNCO) and/or carbon monoxide (CO) after the breakage of the N(1)–C(5) and C(2)–N(3) bonds to yield 2-amino-propanedinitrile (or aminomalonitrile, IX, C₃H₃N₃, formally trimer of the HCN molecule), which is another important molecule in prebiotic nucleobase formation

(Voet & Schwartz 1983; Raulin et al. 1984). Although the formation of IX was also confirmed by the kinetic fits (Section 4.3.2), these are expected to be slow reactions as (contrary to species VIII) it could not be observed either in EI-QMS or via PI-ReTOF-MS. Furthermore, its weak IR absorption peak is likely masked by the dominant species VIII at 2205 cm^{-1} . Other species such as I could also partly account for this nitrile stretching mode besides VIII in the irradiated mixture sample; however, it is assumed to be quickly oxidized into VIII as stated above. This was also corroborated by the kinetic fits (Section 4.3.2).

The carbon monoxide (CO) formed during the radiolysis of the mixture sample can easily be oxidized further, therefore it likely accounts for the formation of carbon dioxide (CO_2) as it was observed in earlier organic radiolysis works as well (Góbi et al. 2016a). Besides, the other irradiation product, isocyanic acid (HNCO), can transform into the isocyanate (OCN^-) anion as shown previously (Broekhuizen et al. 2004). It should be noted that nitrile-bearing compounds ($\text{R}-\text{C}\equiv\text{N}$) were also successfully converted into isocyanates (Hudson & Moore 2004); however, based on the kinetic study (Section 4.3.2) this should be considered a minor pathway only. The last species forming upon irradiation is nitrogen monoxide (NO), which can be detected via the FTIR and PI-ReTOF-MS methods and may have several possible sources. The most likely of these origins is the direct oxidation of the adenine molecule ($\text{C}_5\text{H}_5\text{N}_5$, see Figure 2(f) for the lack of its signal in the mixture sample) or oxidation of hydrogen cyanide (HCN) forming along with species I during the first step of the electron radiolysis scheme of neat adenine, i.e., without oxidation (Figure 3). Alternatively, the oxidation of cyanamide ($\text{H}_2\text{N}-\text{C}\equiv\text{N}$) might also yield nitrogen monoxide (NO); this would explain the decrease in its signal intensity (and that of its fragment; Figures 2(c) and (d)) in the PI-ReTOF-MS spectrum as well. It is highly likely that nitrogen monoxide originates from more than one of the above-mentioned possible sources as it has a bimodal PI-ReTOF-MS TPD profile (Figure 2(e)) with the second peak occurring at the same time as the adenine sublimation event in the neat sample. This implies that this second signal of nitrogen monoxide may be assigned to the oxidation of adenine molecules, which remained intact after the electron irradiation of the mixture sample.

Nitrogen monoxide could also be formed by the oxidation of the imidogen (NH) radicals as the other product of the carbon monoxide (CO) loss of species V, VII, and VIII. However, it would result in a much higher number of nitrogen monoxide molecules in the radiolyzed samples than the experimentally obtained value (see mass balances in Section 4.2.2), as it should be comparable to the number of carbon monoxide molecules that form together with the imidogen radicals. The strongest evidence for the source of nitrogen monoxide (NO) can be given based on the findings of Evans et al. (2011). According to their results, nitrogen monoxide could be observed when molecular oxygen (O_2) was deposited on a pre-irradiated adenine ($\text{C}_5\text{H}_5\text{N}_5$) sample and was irradiated with energetic electrons. As the thickness of the oxygen layer was higher than the penetration depth of the electrons (500 nm), the adenine molecules were not exposed to the energetic electrons; however, ozone (O_3) was formed in the irradiated oxygen ice as detected via the FTIR and EI-QMS methods. This reactive species could then diffuse down to the deeper parts of the sample and react with the products formed during the pre-irradiation of adenine, yielding nitrogen monoxide (NO) along

with other species such as epoxides ($\text{C}-\text{O}-\text{C}$) and organics with a carbonyl functional group ($\text{R}_1\text{R}_2-\text{C}=\text{O}$). This implies that nitrogen monoxide emerges by the oxidation of the species formed during the neat adenine ($\text{C}_5\text{H}_5\text{N}_5$) radiolysis, and its formation does not require the irradiation of the adenine sample itself at the same time, as is the case for the mixture sample.

Although the second pathway (Figure 4) is more likely to occur in the mixture sample, the original radiolysis mechanism (Figure 3) can still take place, allowing for the detection of their products such as cyanamide ($\text{H}_2\text{N}-\text{C}\equiv\text{N}$) as well as the oxidation product nitrogen monoxide (NO). However, as it has been previously pointed out, they can also be oxidized, therefore their concentration in the sample decreases, as can be observed in the PI-ReTOF-MS spectrum of the mixture sample (Figures 2(c) and (d)). This means that although the neat adenine ($\text{C}_5\text{H}_5\text{N}_5$) sample decomposes via a purely radiolytic mechanism that starts with bond breakages and fragmentation (Figure 3), another competing reaction mechanism becomes dominant in the presence of perchlorates (ClO_4^-)—the one involving oxidation reactions as the first (and later) reaction step(s) according to Figure 4.

4.2. Mass Balances

4.2.1. Neat Adenine Samples

The number and percentage of the decomposed adenine ($\text{C}_5\text{H}_5\text{N}_5$) in both the neat and mixture samples can be evaluated based on their infrared absorption bands (Table 5) and depicts a first-order exponential decay fitted via Equation (1):

$$I(t) = I(0)e^{-k_i t}, \quad (1)$$

where $I(t)$ is the number of the molecules' band area (cm^{-1}) at a given time (t , in s), $I(0)$ is the band area at the beginning of the radiolysis (cm^{-1}), and k_i is the decay rate constant of the i th vibrational mode that is to be determined (s^{-1}). Once the k_i values are obtained by fitting, the ratio of the decomposed molecules to the number of exposed ones (i.e., $I_i(60)/I_i(0)$) can be calculated and averaged over all IR vibrational modes. Since the number of exposed adenine molecules is also known ($(2.01 \pm 0.43) \times 10^{17}$), the absolute number of decomposed ones can also be calculated ($(1.80 \pm 0.39) \times 10^{17}$). By comparing these two numbers to each other, it can be concluded that $89.4\% \pm 4.9\%$ of the exposed adenine molecules decayed in the neat sample. Since the exact structure of the forming organic nitrile ($\text{R}-\text{C}\equiv\text{N}$, likely caused by species I, II, III, and IV) and therefore the integrated absorption coefficient of its vibrational band at 2213 cm^{-1} is unknown, the number of molecules in the sample cannot be determined.

4.2.2. Adenine–Magnesium Perchlorate Hexahydrate Samples

The corresponding values for the adenine ($\text{C}_5\text{H}_5\text{N}_5$)–magnesium perchlorate hexahydrate ($\text{Mg}(\text{ClO}_4)_2 \cdot 6\text{H}_2\text{O}$) 1:1 mixture sample are $(5.99 \pm 1.26) \times 10^{16}$ and $(6.05 \pm 1.27) \times 10^{16}$ indicating that practically all adenine molecules ($99.1\% \pm 1.3\%$) were destroyed within the penetration depth of the electrons. When comparing it to the value obtained for the neat sample (Section 4.2.1), it can be firmly concluded that the presence of the oxidizing agent enhances the destruction of the organic compound, which is in complete accordance with the findings of previous similar studies with organics (Góbi et al. 2016a, 2017). The number of destroyed

Table 5
Mass Balance of the Neat Adenine and the Adenine–Mg(ClO₄)₂ · 6H₂O 1:1 Samples as well as that of the Irradiation Products Determined from their Experimental IR Decay/Growth Curves

Process	Decay Product	Number of Molecules Produced/Decomposed During Irradiation	
		Adenine	Adenine–Mg(ClO ₄) ₂ · 6H ₂ O
C ₅ H ₅ N ₅ → X		(1.80 ± 0.39) × 10 ¹⁷	(5.99 ± 1.26) × 10 ¹⁶
Fraction of adenine degraded		89.4% ± 4.9%	99.1% ± 1.3%
ClO ₄ [−] → ClO ₃ [−] + O	O	...	(4.52 ± 0.95) × 10 ¹⁷ ^d
H ₂ O → 2H + O			(5.16 ± 1.09) × 10 ¹⁷ ^b
Number of molecules in sample after irradiation	C ₄ H ₄ N ₄ O (VIII) ^a	...	(4.06 ± 0.26) × 10 ¹⁶
	CO	...	(2.88 ± 0.19) × 10 ¹⁶
	HNCO	...	(2.85 ± 0.19) × 10 ¹⁶
	CO ₂	...	(2.72 ± 0.18) × 10 ¹⁶
	OCN [−]	...	(1.27 ± 0.38) × 10 ¹⁵
	NO	...	(1.47 ± 0.73) × 10 ¹⁴
	Carbon balance ^b	...	67.0 ± 15.1%
	Nitrogen balance ^b	...	64.2% ± 14.2%
	Oxygen balance ^c	...	34.0% ± 7.5% ^d
			29.8% ± 5.8% ^e

Notes.

^a C₄H₄N₄O corresponds to species VIII in Figure 4.

^b Fraction of carbon or nitrogen atoms originating from adenine destruction that are needed for radiolysis product formation.

^c Fraction of oxygen atoms originating from adenine and crystalline water destruction that are needed for radiolysis product formation.

^d If the reaction ClO₄[−] → ClO₃[−] + O is regarded exclusively besides the destruction of water.

^e If the reaction ClO₃[−] → ClO₂[−] + O is also considered.

magnesium perchlorate hexahydrate (Mg(ClO₄)₂ · 6H₂O) molecules can also be determined besides the exposed ones; these are (6.41 ± 1.35) × 10¹⁶ and (6.47 ± 1.36) × 10¹⁶, i.e., (99.0% ± 2.1%) of the exposed molecules were decayed within the penetration depth of the electrons.

Since the integrated band areas and absorption coefficients are known for the forming species, their number in the sample can also be estimated (Table 5); for instance, for the carbon dioxide (CO₂), the signal at 2342 cm^{−1} is 7.6 × 10^{−17} cm molecule^{−1} (Gerakines et al. 1995), resulting in (2.72 ± 0.18) × 10¹⁶ molecules in the sample after irradiation. These are 7.8 × 10^{−17} cm molecule^{−1} (Lowenthal et al. 2002) and therefore (2.85 ± 0.19) × 10¹⁶ molecules for isocyanic acid (HNCO, 2252 cm^{−1}), 1.3 × 10^{−16} cm molecule^{−1} for the cyanate ion (OCN[−], 2168 cm^{−1}) (Broekhuizen et al. 2004) meaning (1.27 ± 0.38) × 10¹⁵ molecules, 1.1 × 10^{−17} cm molecule^{−1} for carbon monoxide (CO, 2139 cm^{−1}) (Gerakines et al. 1995) accounting for (2.88 ± 0.19) × 10¹⁶ molecules, and 6.8 × 10^{−18} cm molecule^{−1} for nitrogen monoxide (NO, 1870 cm^{−1}) (Stirling et al. 1994) corresponding to (1.47 ± 0.73) × 10¹⁴ molecules in the sample. Note that the number of nitrogen monoxide molecules is two orders of magnitude lower than that of the carbon monoxide molecules confirming that the former could not be formed via the oxidation of imidogen (NH) radicals forming as co-product of the CO loss (Section 4.1.2). Although the absorption coefficient of species VIII (C₄H₄N₄O) for its carbonyl stretching vibration (ν C=O) at around 1749 cm^{−1} is unknown, it should be similar to other aldehydes/ketones that have absorption coefficients in the range of 1.4–1.8 × 10^{−17} cm molecule^{−1} (Kaiser et al. 2014). Therefore, the assumption of a value of (1.6 ± 0.2) × 10^{−17} cm molecule^{−1}, which is equal to (4.06 ± 0.26) × 10¹⁶ molecules in the irradiated sample, is straightforward; this is in agreement with the findings of the kinetic study as well (Section 4.3.2).

By adding up the number of carbon, nitrogen, and oxygen atoms in these species, one can compare them to the total number of these elements originating from the decayed adenine (C₅H₅N₅) or—in the case of oxygen atoms (O)—from the magnesium perchlorate hexahydrate (Mg(ClO₄)₂ · 6H₂O) molecules. The formation of carbon dioxide (CO₂), isocyanic acid (HNCO), cyanate ion (OCN[−]), carbon monoxide (CO), nitrogen monoxide (NO), and species VIII requires (2.01 ± 0.16) × 10¹⁷ carbon and (1.92 ± 0.13) × 10¹⁷ nitrogen atoms. These two account for the 67.0% ± 15.1% and 64.2% ± 14.2% of the total number of carbon and nitrogen atoms originating from the decomposed adenine (C₅H₅N₅) molecules. Note that both the total resource of carbon and nitrogen atoms equal (3.00 ± 0.63) × 10¹⁷, as every adenine molecule has five of each. If it is assumed that every destroyed perchlorate unit (ClO₄[−]) yields only one oxygen atom (O), then the number of the latter produced is much lower than the number required for the formation of the above-mentioned species (cf. (6.41 ± 1.35) × 10¹⁶ and (1.54 ± 0.10) × 10¹⁷). Alternatively, one might also investigate that the radiolysis product chlorate (ClO₃[−]) may be decayed further into chlorite (ClO₂[−]) meaning that one irradiated perchlorate unit yields two oxygen atoms. However, even if it were assumed that all chlorates transform to chlorites completely, it would result in (1.28 ± 0.27) × 10¹⁷ oxygen atoms, which is still below the number required for the formation of the products discussed above and cannot explain the huge molecular oxygen (O₂) signal that can be observed in the EI-QMS TPD at about 55K (Figure 2(a)), therefore another source of oxygen must be present as well. This contradiction can be resolved if the oxygen atoms of the crystalline water molecules are also taken into account; as every magnesium perchlorate has six crystalline water molecules, the total oxygen resource easily offsets the required number of oxygen atoms. This seemingly contradicts the findings of Turner et al. (2016) since they found that the oxygen originates exclusively from the perchlorate unit (ClO₄[−]). However, it must be pointed out that the

dose used for this current experiment was approximately 20 times higher (820 ± 180 versus 39 ± 2 eV/(Mg(ClO₄)₂ · 6H₂O) molecule), which may be high enough to destroy the water molecules surrounding the perchlorate units. Moreover, the formation of molecular oxygen (O₂) was previously observed in irradiated water ices (H₂O; Zheng et al. 2006a and 2006b). This approach still assumes that the perchlorate unit loses only one oxygen atom to yield chlorates (ClO₃⁻).

Evidence for crystalline water destruction can be found in the FTIR spectrum, where the gradual decrease of the water antisymmetric (ν_{as} OH, 3617 cm⁻¹) and symmetric (ν_s OH, 3567 and 3546 cm⁻¹) stretching vibrations can be observed, implying that the crystalline water was also completely destroyed within the penetration depth of the electrons upon irradiation. This means $(3.88 \pm 0.82) \times 10^{17}$ water molecules decayed, resulting in the new value of the total oxygen resource $((4.52 \pm 0.95) \times 10^{17}$ atoms), meaning that the species formed account for the 34.0% ± 7.5% of oxygen atoms (O) originating from both the perchlorate (ClO₄⁻) unit as well as the crystalline water (H₂O). It should be noted that the total oxygen resource equals $(5.16 \pm 1.09) \times 10^{17}$ oxygen atoms if the complete destruction of chlorates (ClO₃⁻) further into chlorites (ClO₂⁻) is also investigated. In this case, the species discussed above would account for the 29.8% ± 5.8% of the oxygen atoms formed upon irradiation. Unfortunately, the number of oxygen molecules in the sample cannot be quantified by their weak IR stretching signal at 1550 cm⁻¹ (Vandenbussche et al. 1999) as it is completely masked by the huge absorption band of the reactant adenine, therefore it cannot be decided which of the alternatives regarding the oxygen source described above are more likely to occur.

The unreacted oxygen then sublimes during the TPD and leaves the sample at 55 K as molecular oxygen (O₂); they can be detected via EI-QMS (Figure 2(a)). It is worth noting that this peak has a considerably larger signal strength than the other oxygen peaks at higher temperatures as the latter might be caused by the oxygen related to the thermal degradation of various metastable chlorine oxide (Cl_xO_y) compounds formed upon the electron irradiation of the sample (see also Section 3.2 and Góbi et al. 2016b). Lastly, an estimate of the number of chlorine dioxide molecules can also be given based on the PI-ReTOF-MS signals. The integrated ion counts of nitrogen monoxide (NO) and chlorine dioxide (³⁵ClO₂) peaks are known (812 and 5277) as well as their photoionization cross-section at the photoionization energy of 10.49 eV (2.74×10^{-18} cm² (Watanabe et al. 1967) and 5×10^{-18} cm² (Flesch et al. 1999)). If the integrated ion counts of chlorine dioxide is corrected by the ratio of the ionization cross-sections yielding 2892, then the number of molecules can be calculated by knowing the number of nitrogen monoxide molecules in the sample ($(1.47 \pm 0.73) \times 10^{14}$); the value of $(5.24 \pm 0.26) \times 10^{14}$ can be obtained, making up 8.2% ± 2.1% of the number of perchlorate units (ClO₄⁻) destroyed. It is important to note, however, that since the other chlorine-bearing molecules cannot be quantified, in contrast to carbon, nitrogen, and oxygen, the mass balance cannot be given for chlorine. Furthermore, quantitative information cannot be extracted from the EI-QMS due to the peak saturation at 55 K, which hinders the correct integration of signals.

4.3. Adenine Destruction Rates and Product Formation Rates

4.3.1. Neat Adenine Samples

The integrated IR band areas of the adenine (C₅H₅N₅) in both samples gradually decrease upon irradiation, and one selected signal (that of the ν CN(R6) and ν CC(R6) vibrational modes at around 1600 cm⁻¹) is plotted in Figures 5(a) and 6(a). The change in band area versus time is also plotted for the magnesium perchlorate hexahydrate (Mg(ClO₄)₂ · 6H₂O); in this case the selected signal was the broad band between 1200 and 900 cm⁻¹ (the ν_{as} ClO₄⁻ and ν_{as} ClO₄⁻ vibrational modes); this is displayed in Figure 6(b). All of these show a (pseudo) first-order radiolytic decay, meaning that the data points can be fitted with Equation (1). The decay rate constant determined for the neat adenine (C₅H₅N₅) sample with a mechanism summarized in Figure 3 in Section 4.1.1 is found to be $(2.20 \pm 0.53) \times 10^{-4}$ s⁻¹, which is in good agreement with the one obtained by Evans et al. (2011) at the same temperature ($(1.65 \pm 0.37) \times 10^{-4}$). The kinetic profile of the sole irradiation product, the alkyl nitrile compound (R-C≡N at 2213 cm⁻¹, possibly caused by species I, II, III, and IV, Figure 5(b)), can be fitted with the growth curve (2):

$$I_{R-C\equiv N, 2210 \text{ cm}^{-1}}(t) = A(1 - e^{-k_i t}), \quad (2)$$

where A is a constant and it is proportional to the number of adenine (C₅H₅N₅) molecules in the sample. Its formation rate constant (k_i) is equal to $(7.47 \pm 3.10) \times 10^{-5}$ s⁻¹, which also compares to the value of this irradiation product according to Evans et al. (2011) ($(4.53 \pm 0.58) \times 10^{-5}$ s⁻¹).

4.3.2. Adenine–Magnesium Perchlorate Hexahydrate Samples

The pseudo first-order decomposition rate constant of adenine (C₅H₅N₅) for the mixture sample is $(5.08 \pm 1.30) \times 10^{-4}$ s⁻¹, i.e., a more than twofold increase in the decay rate constant when the oxidizing agent is present in the sample. This corresponds to a half-life of adenine of approximately 6.5×10^7 years upon bombardment by GCR particles at 2–3 cm below the surface (or 6.5×10^8 years in the depth of 5–10 cm; Pavlov et al. 2012). It should be noted that this is comparable to the rate of hydrolysis by the thin water films in the shallow subsurface at the average Martian temperatures of 250 K (Levy & Miller 1998). The relative increase in the reaction rate constant at 10 K in the presence of perchlorates is comparable to the one found for glycine–magnesium perchlorate hexahydrate (Mg(ClO₄)₂ · 6H₂O) mixtures (+99% ± 26%, Góbi et al. 2016a). This can be explained by the well-investigated decomposition of perchlorates (ClO₄⁻) into atomic oxygen (O, Turner et al. 2016) and other oxidants such as chlorine dioxide (ClO₂, Góbi et al. 2016b), which then can react with the surrounding organic molecules enhancing their radiolytic decomposition. As has been mentioned already, the destruction rate constant of the perchlorate units (ClO₄⁻) can also be evaluated using Equation (1), and it is found to be $((4.30 \pm 0.54) \times 10^{-4}$ s⁻¹).

In order to determine the formation rate constants of the irradiation products, such as carbon dioxide (CO₂), isocyanic acid (HNCO), cyanate anion (OCN⁻), carbon monoxide (CO), and species VIII (C₄H₄N₄O), the first-order kinetic fit cannot be applied as they take part in multiple complex, higher-order reactions. This is also reflected in their kinetic profiles, if plotted (Figures 6(c)–(g)), which do not follow the growth curve (Equation (2)) in contrast to the only irradiation product species R-C≡N of the neat adenine (C₅H₅N₅) sample. By utilizing a set

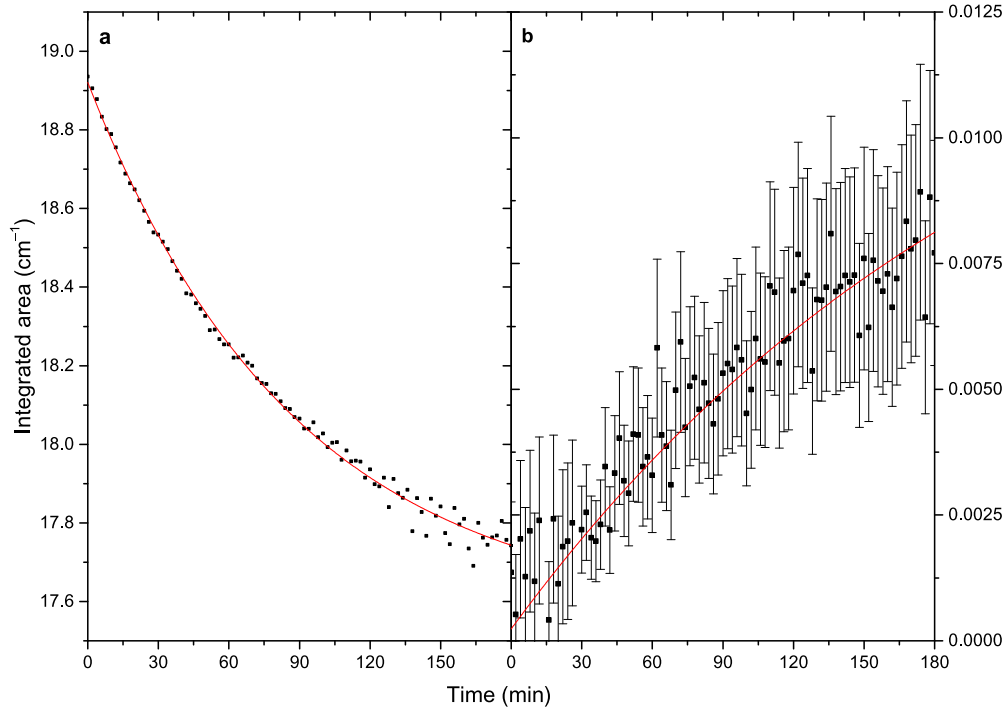


Figure 5. (a) Decay curve of the IR band at 1619–1600 cm⁻¹ (ν CN(R6) and ν CC(R6) vibrations of the adenine molecule) and (b) growth curve of the IR band at 2213 cm⁻¹ (ν CN vibration of species “R-CN”) of the neat adenine sample upon energetic electron irradiation.

Table 6
Decay Rate Constants (in s⁻¹) of the Neat Adenine and the Adenine–Mg(ClO₄)₂ · 6H₂O 1:1 Samples as well as the Formation Rates of the Irradiation Products Based on their Experimental IR Decay/Growth Curves

Number	Reaction	Rate Constant	Value ^a	(Pseudo) First-order Value
R1	C ₅ H ₅ N ₅ + O → V	k_1	$(6.12 \pm 0.25) \times 10^{-16}$	$(2.78 \pm 0.11) \times 10^{-4}$
R2	V + O → VII	k_2	$(3.79 \pm 0.93) \times 10^{-14}$	$(1.72 \pm 0.42) \times 10^{-2}$
R3	V → HNCO + I	k_3	...	$(1.64 \pm 1.58) \times 10^{-2}$
R4	V → CO + I + NH	k_4	...	$(1.48 \pm 1.11) \times 10^{-2}$
R5	I + O → VIII	k_5	$(5.52 \pm 1.67) \times 10^{-16}$	$(2.51 \pm 0.76) \times 10^{-4}$
R6	VII → HNCO + VIII	k_6	...	$(2.41 \pm 0.33) \times 10^{-4}$
R7	VII → CO + VIII + NH	k_7	...	$(3.42 \pm 0.03) \times 10^{-4}$
R8	VIII → CO + IX + NH	k_8	...	$(5.36 \pm 0.09) \times 10^{-5}$
R9	HNCO → OCN ⁻ + H ⁺	k_9	...	$(7.31 \pm 0.07) \times 10^{-6}$
R10	CO + O → CO ₂	k_{10}	$(3.16 \pm 0.83) \times 10^{-16}$	$(1.44 \pm 0.38) \times 10^{-4}$
R11	Mg(ClO ₄) ₂ · 6H ₂ O → Mg(ClO ₃) ₂ · 6H ₂ O + O	k_{11}	...	$(3.83 \pm 0.01) \times 10^{-4}$

Note.

^a Second-order reaction rates; its corresponding pseudo first-order rate can also be obtained (see main text).

of 11 coupled differential equations according to the proposed decay mechanism of adenine in the presence of magnesium perchlorate hexahydrate (Mg(ClO₄)₂ · 6H₂O, Section 4.1.2), they can be fitted numerically (Frenklach et al. 1992); all the equations and the resulting formation rate constants are summarized in Table 6. After solving these equations, it can be seen that the destruction of the perchlorate molecule (reaction R11) follows a unimolecular decay and its rate constant (k_{11}) is found to be $(3.83 \pm 0.01) \times 10^{-4}$ s⁻¹, which is within the uncertainty limits of the value determined with the use of Equation (1) $((4.30 \pm 0.54) \times 10^{-4}$ s⁻¹). In contrast to this, as the adenine (C₅H₅N₅) molecule reacts with oxygen (reaction R1) while being oxidized to species V, it takes part in a bimolecular reaction, which has a rate constant of $(6.12 \pm 0.25) \times 10^{-15}$ s⁻¹ (k_1).

According to R1, it can also be concluded that the pseudo (or apparent) first-order rate constant (k'_1) can be obtained by multiplying k_1 with the average number of free oxygen atoms in the sample ($n[\text{O}]_{\text{av}} = (4.54 \pm 2.90) \times 10^{11}$) according to the steady-state approximation. It is also important to note that since the number of oxygen atoms at a given time could not be measured directly by the experimental methods used, and furthermore, due to the fact that the differential equation solver can only determine their product k'_1 , both the values of k_1 and $n[\text{O}]_{\text{av}}$ do not have real physical meaning. Moreover, the higher-order and pseudo first-order values have the same units (both are given in s⁻¹) as the number of molecules is a dimensionless value. Nevertheless, k'_1 does have a physical meaning and its value can be calculated: $k'_1 = (2.78 \pm 0.11) \times 10^{-4}$ s⁻¹.

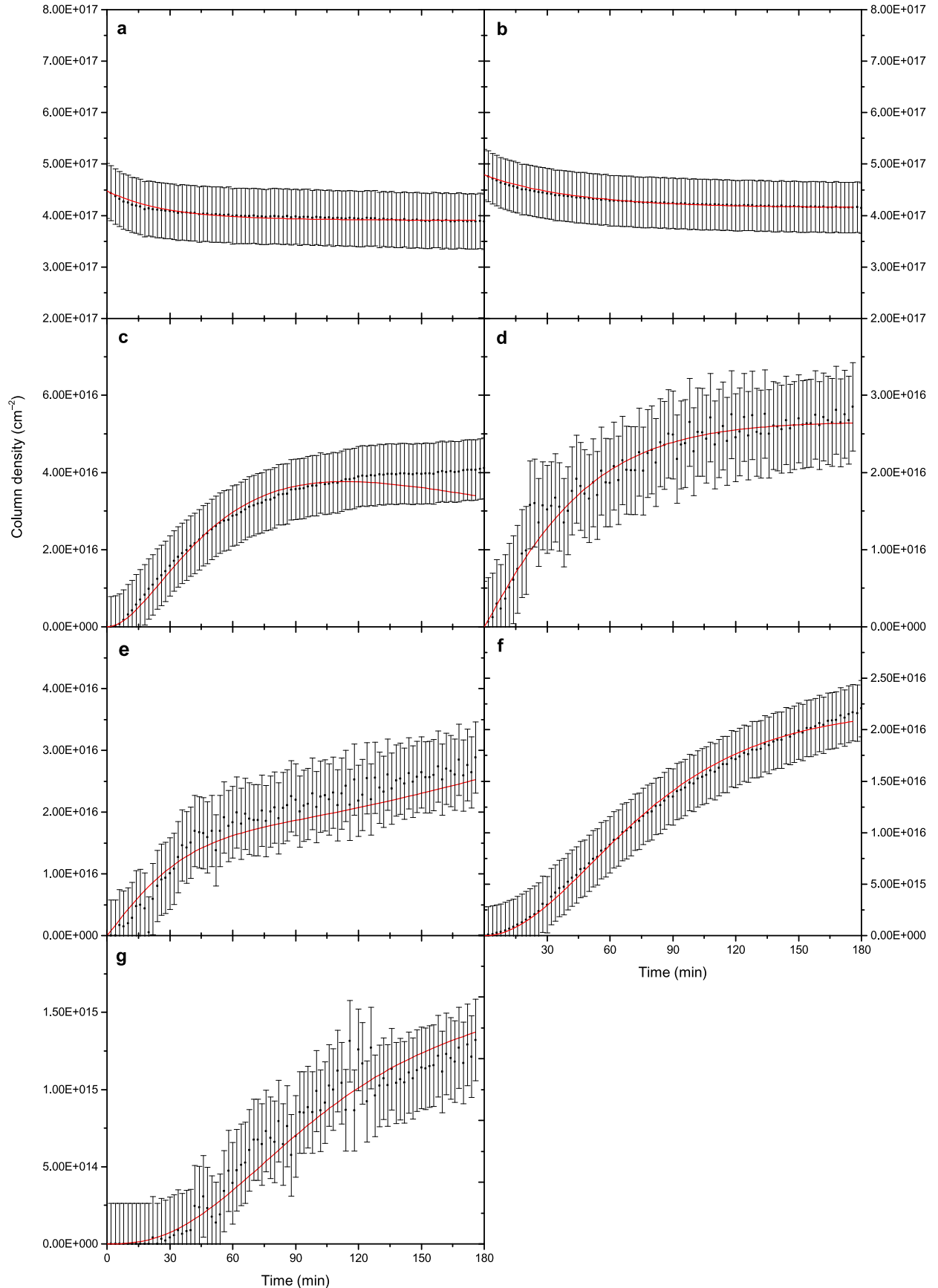


Figure 6. Decay curves of the IR bands (a) at $1628\text{--}1578 \text{ cm}^{-1}$ ($\nu \text{CN(R6)}$ and $\nu \text{CC(R6)}$ vibrations of the adenine molecule, respectively), (b) at $1119\text{--}954 \text{ cm}^{-1}$ ($\nu_{\text{as}} \text{ClO}_4^-$ and $\nu_s \text{ClO}_4^-$ vibrations of the $\text{Mg}(\text{ClO}_4)_2 \cdot 6\text{H}_2\text{O}$ molecule), growth curves of the IR bands (c) at 1749 cm^{-1} ($\nu \text{C=O}$ vibration of the $\text{C}_4\text{H}_4\text{N}_4\text{O}$, molecule VIII), (d) at 2252 cm^{-1} ($\nu_{\text{as}} \text{N=C=O}$ vibration of the HNCO molecule), (e) 2139 cm^{-1} (νCO vibration of the CO molecule), (f) 2342 cm^{-1} ($\nu_{\text{as}} \text{CO}_2$ vibration of the CO₂ molecule), (g) 2165 cm^{-1} ($\nu_{\text{as}} \text{OCN}^-$ vibration of the OCN⁻ ion) of the adenine- $\text{Mg}(\text{ClO}_4)_2 \cdot 6\text{H}_2\text{O}$ 1:1 mixture sample upon energetic electron irradiation.

According to the decomposition scheme in Figure 4 (Section 4.1.2), V can be oxidized into species VII (R2); alternatively, it transforms into I either after the loss of isocyanic acid (HNCO, R3) or carbon monoxide (CO, R4) molecules, respectively. The second-order reaction rate constant for R2 is obtained to be $k_2 = (3.79 \pm 0.93) \times 10^{-14} \text{ s}^{-1}$ ($k'_2 = (1.72 \pm 0.42) \times 10^{-2} \text{ s}^{-1}$), whereas the same values for R3 and R4 are equal to $k_3 = (1.64 \pm 1.58) \times 10^{-2} \text{ s}^{-1}$ and $k_4 = (1.48 \pm 1.11) \times 10^{-2} \text{ s}^{-1}$, respectively. Therefore, all of them can be regarded as reactions occurring rapidly. Similarly to R2, the reaction of an active oxygen atom (O) with I yields species VIII (R5), having a rate constant of $k_5 = (5.52 \pm 1.67) \times 10^{-16} \text{ s}^{-1}$ ($k'_5 = (2.51 \pm 0.76) \times 10^{-4} \text{ s}^{-1}$), whereas VII can have the same decomposition steps as molecule V in reactions R3 and R4, leading to the formation of isocyanic acid (HNCO, R6, $k_6 = (2.41 \pm 0.33) \times 10^{-4} \text{ s}^{-1}$) and carbon monoxide (CO, R7, $k_7 = (3.42 \pm 0.03) \times 10^{-4} \text{ s}^{-1}$). It is worth noting, however, that the rate constants of R5, R6, and R7 are about two orders of magnitude smaller than those of R2, R3, and R4. Furthermore, similarly to R4 and R7, R8 also leads to the formation of carbon monoxide (CO) and species IX from VIII ($k_8 = (5.36 \pm 0.09) \times 10^{-5} \text{ s}^{-1}$). Species VIII therefore has three different sources (R5, R6, and R7) but only one relevant decomposition mechanism (R8) with a relatively small reaction rate constant, allowing for the detection of the latter molecule via the FTIR method (Section 3.1.2).

The isocyanic acid (HNCO) formed in reactions R3 and R6 can be further transformed into cyanate anion (OCN^- , R9), and both can be detected by their FTIR signals (Section 3.1.2); this is the only mechanism that can account for the loss of the former species having an apparently small rate constant ($k_9 = (7.31 \pm 0.07) \times 10^{-6} \text{ s}^{-1}$). The carbon monoxide (CO) molecule can evidently be oxidized to carbon dioxide (CO_2 , R10). The formation rate constant of the latter can also be estimated by solving the coupled differential equations: $k_{10} = (3.16 \pm 0.83) \times 10^{-16} \text{ s}^{-1}$ ($k'_{10} = (1.44 \pm 0.38) \times 10^{-4} \text{ s}^{-1}$; this is in good agreement with the values obtained for various glycine–magnesium perchlorate hexahydrate ($\text{Mg}(\text{ClO}_4)_2 \cdot 6\text{H}_2\text{O}$) samples ($(2.55 \pm 0.17) \times 10^{-4} \text{ s}^{-1}$ and $(3.06 \pm 0.20) \times 10^{-4} \text{ s}^{-1}$ (Góbi et al. 2017)). Furthermore, according to Figure 4 and Section 4.1.2, adenine ($\text{C}_5\text{H}_5\text{N}_5$) is oxidized on carbon atom C(2) at first and then C(8); this finding is also confirmed by the kinetic studies. Namely, if a new kinetic pathway with the derivative of V (with an oxygen on C(8) instead of on C(2), i.e., 8-oxo-adenine, VI, $\text{C}_5\text{H}_5\text{N}_5\text{O}$) is included in the coupled differential equations, then its formation rate constant (k_{1a}) is found to be approximately 20 times smaller than k_1 . The same holds true for the isocyanic acid (HNCO)-loss reaction of species VIII and for the possible isocyanate (OCN^-) formation from molecules containing a nitrile group (R-C≡N; (Hudson & Moore 2004)) as competing reaction pathways with R8 and R9; if they are implemented into the coupled differential equations, their obtained rate constants are two to three orders of magnitude smaller, making them negligible compared to the main decomposition routes. These findings justify the omission of these minor pathways from the decomposition scheme described in Figure 4 and are in accordance with the FTIR, PI-ReTOF-MS, and EI-QMS results (Section 3) as well.

5. Astrophysical Implications

The aim of the present work was to unravel the radiolysis of the astrobiologically relevant nucleobase adenine ($\text{C}_5\text{H}_5\text{N}_5$) molecule—formally the pentamer of hydrogen cyanide (HCN)—in the presence of oxidants, namely magnesium perchlorate hexahydrate ($\text{Mg}(\text{ClO}_4)_2 \cdot 6\text{H}_2\text{O}$). Perchlorates are abundant on the Martian surface, therefore they represent relevant species that may facilitate the decomposition rate of organic molecules upon irradiation, which can explain their lower-than-expected concentration in the Martian subsurface as it has been shown previously (Góbi et al. 2016a). Neat adenine and adenine–magnesium perchlorate hexahydrate 1:1 mixtures were irradiated with energetic electrons that mimic the secondary electrons originating from the interaction between GCR particles and the constituents of the Martian surface. The radiolysis of the samples were probed online and in situ via the FTIR method, then their TDP profiles were monitored by means of the PI-ReTOF-MS instrument; EI-QMS spectra of the samples were also collected throughout the experiment as well. The experimental work was supplemented by Monte Carlo (CASINO) simulations that allowed calculating the average dose a molecule absorbs within the average penetration depth of the electrons. According to these, the average dose corresponded to approximately 650 Myr of exposure to GCRs 2–3 cm below the Martian surface.

The use of the PI-ReTOF-MS aside from the classical FTIR and EI-QMS methods allowed us to untangle the radiolytic degradation mechanism of the neat adenine ($\text{C}_5\text{H}_5\text{N}_5$) and its mixture with magnesium perchlorate hexahydrate ($\text{Mg}(\text{ClO}_4)_2 \cdot 6\text{H}_2\text{O}$) upon electron irradiation in detail. As a result it can be concluded that the first decomposition step of the neat adenine sample is a loss of hydrogen cyanide (HCN) that can later attack the neighboring adenine molecules and take part in a nucleophile substitution yielding the cyano-derivatives of adenine as it has been pointed out previously (Evans et al. 2011). The other product molecule of the HCN loss of adenine is 1H-5-aminoimidazol-4-carbonitrile (I), which is formally the HCN tetramer and has been shown to have an important role in the prebiotic synthesis of adenine. This species can further decompose upon irradiation, losing a carbodiimide (HNCNH) unit that quickly rearranges into its more stable form cyanamide ($\text{H}_2\text{N}-\text{C}\equiv\text{N}$), which later can be detected via the PI-ReTOF-MS method. All of these may account for the R-C≡N vibrational feature emerging upon irradiation as can be monitored by the help of the FTIR spectroscopy. The decay profile of adenine as well as the growth profile of this new R-C≡N signal could also be fitted using (pseudo) first-order kinetics.

When irradiated in the presence of perchlorates (ClO_4^-), adenine ($\text{C}_5\text{H}_5\text{N}_5$) is decomposed into a plethora of radiolysis products such as carbon dioxide (CO_2), nitrogen monoxide (NO), isocyanate anion (OCN^-), isocyanic acid (HNCO), and carbon monoxide (CO), as could be observed in the FTIR spectrum of the mixture sample. The already-known irradiation products of perchlorates, molecular oxygen (O_2) and chlorine dioxide (ClO_2), could also be monitored by EI-QMS and PI-ReTOF-MS (Góbi et al. 2016b; Turner et al. 2016). The presence of these new products as well as the lowered concentration of cyanamide ($\text{H}_2\text{N}-\text{C}\equiv\text{N}$) both suggest that a new decomposition mechanism involving oxidation reactions

becomes the predominant one. The growth profiles of the products listed above do not follow a simples (pseudo) first-order kinetics, therefore a set of 11 coupled differential equations had to be solved numerically. This helped determine the exact decomposition mechanism of adenine in the presence of oxidizing agents and also allowed the molecule 1H-5-aminoimidazol-2-oxo-4-carbonitrile (VIII, $C_4H_4N_4O$), which has been undetected so far and may account for the new vibrational features in the R-C≡N and $R_1R_2-C=O$ stretching region, to be unraveled. This mechanism also includes molecules that are well-known oxidation products of adenine, for instance 2-oxo-adenine (or isoguanine, V, $C_5H_5N_5O$) and 2,8-dioxo-adenine (VII, $C_5H_5N_5O_2$) and a species that is important in the prebiotic synthesis of adenine such as 2-amino-propanedinitrile (or aminomalonitrile, IX, $C_3H_3N_3$, formally trimer of the HCN molecule). When calculating the mass balance, one can find that all these products account for roughly 60% of the both the carbon and nitrogen and 30% of the oxygen atoms formed upon the destruction of adenine ($C_5H_5N_5$) in the mixture sample. The rest of the oxygen leaves the sample as unreacted molecular oxygen (O_2), which can be observed via the EI-QMS instrument. The assumption that the perchlorate unit (ClO_4^-) loses only one oxygen, yielding chlorates (ClO_3^-), does not provide enough oxygen atoms, therefore it has to be taken into account that they must originate from the decomposition of crystalline water of magnesium perchlorate hexahydrate ($Mg(ClO_4)_2 \cdot 6H_2O$) as well. This may seem to be in contradiction with earlier results (Turner et al. 2016) but the high doses used by the current work may explain this apparent discrepancy. Alternatively, the decomposition of radiolysis product chlorates (ClO_3^-) yielding further oxygen atoms can also partly account for the oxygen mass balance.

In contrast to the fact that adenine ($C_5H_5N_5$) has been extensively studied by the astrobiology community in the past few decades, many issues have remained unanswered until now. The present work has successfully detected electron irradiation products of this nucleobase for the first time. These species may have a huge impact on the current knowledge on the oxidizing agents on Mars. Furthermore, it represents the first systematic investigation of the decomposition mechanism with the decomposition/formation rate constants of adenine and its radiolysis products in the absence and presence of Martian-relevant oxidizer perchlorates, further extending our view on the radiolytic processes on Mars.

This work was supported by the National Aeronautics and Space Administration under Grant NNX14AG39G.

References

- Abplanalp, M. J., Borsuk, A., Jones, B. M., & Kaiser, R. I. 2015, *ApJ*, 814, 45
 Acuña, M. H., Connerney, J. E. P., Ness, N. F., et al. 1999, *Sci*, 284, 790
 Armstrong, J. C., Leovy, C. B., & Quinn, T. 2004, *Icar*, 171, 255
 Barbatti, M., Borin, A. C., & Ullrich, S. 2015, *Top. Curr. Chem.*, 355, 1
 Bennett, C. J., Ennis, C. P., & Kaiser, R. I. 2014, *ApJ*, 782, 63
 Bennett, C. J., Jones, B., Knox, E., et al. 2010, *ApJ*, 723, 641
 Biemann, K., & Bada, J. L. 2011, *JGRE*, 116, E12001
 Biemann, K., Oró, J., Toulmin, P., et al. 1976, *Sci*, 194, 72
 Bishop, J. L., Quinn, R., & Dyar, M. D. 2014, *AmMin*, 99, 1580
 Botta, O., & Bada, J. L. 2002, *SGeo*, 23, 411
 Broekhuizen, F. A., Keane, J. V., & Schutte, W. A. 2004, *A&A*, 415, 425
 Callahan, M. P., Burton, A. S., Elsila, J. E., et al. 2013, *M&PS*, 48, 786
 Callahan, M. P., Smith, K. E., Cleaves, H. J., II, et al. 2011, *PNAS*, 108, 13995
 Carrier, B. L., & Kounaves, S. P. 2015, *GeoRL*, 42, 3739
 Chen, L., Brédy, R., Bernard, J., et al. 2011, *JChPh*, 135, 114309
 Chevrier, V. F., Hanley, J., & Altheide, T. S. 2009, *GeoRL*, 36, L10202
 Cleaves, H. J., II, Nelson, K. E., & Miller, S. L. 2006, *NW*, 93, 228
 Cockell, C. S., & Raven, J. A. 2004, *Icar*, 169, 300
 Dartnell, L. R., Desorgher, L., Ward, J. M., & Coates, A. J. 2007, *GeoRL*, 34, L02207
 Davila, A. F., Willson, D., Coates, J. D., & McKay, C. P. 2013, *IJAsB*, 12, 321
 Drouin, D., Couture, A. R., Joly, D., et al. 2007, *Scanning*, 29, 92
 Ebata, T., Anezaki, Y., Fujii, M., Mikami, N., & Ito, M. 1983, *JPhCh*, 87, 4773
 Erman, P., Karwajczyk, A., Rachlew-Kallne, E., et al. 1993, *CPL*, 215, 173
 Evans, N. L., Bennett, C. J., Ullrich, S., & Kaiser, R. I. 2011, *ApJ*, 730, 69
 Fateley, W. G., Bent, H. A., & Crawford, B., Jr. 1959, *JChPh*, 31, 204
 Flesch, R., Schürmann, M. C., Plenge, J., et al. 1999, *PCCP*, 1, 5423
 Flynn, G. J. 1996, *EM&P*, 72, 469
 Fornaro, T., Brutac, J. R., Pace, E., et al. 2013, *Icar*, 226, 1068
 Freissinet, C., Glavin, D. P., Mahaffy, P. R., et al. 2015, *JGRE*, 120, 495
 Fenklaich, M., Wang, H., & Rabinowitz, M. J. 1992, *PrECS*, 18, 47
 Gerakines, P. A., Schutte, W. A., Greenberg, J. M., & van Dishoeck, E. F. 1995, *A&A*, 296, 810
 Glavin, D. P., Freissinet, C., Miller, K. E., et al. 2013, *JGRE*, 118, 1955
 Góbi, S., Abplanalp, M. J., & Kaiser, R. I. 2016a, *ApJ*, 822, 8
 Góbi, S., Bergantini, A., & Kaiser, R. I. 2016b, *ApJ*, 832, 164
 Góbi, S., Förstel, M., Maksyutenko, P., & Kaiser, R. I. 2017, *ApJ*, 835, 241
 Guan, Y. Y., Fray, N., Coll, P., et al. 2010, *P&SS*, 58, 1327
 Guimon, C., Khayar, S., Gracian, F., Begtrup, M., & Pfister-Guillouzo, G. 1989, *CP*, 138, 157
 Hanley, J., Chevrier, V. F., Barrows, R. S., Swaffer, C., & Altheide, T. S. 2015, *JGRE*, 120, 1415
 Hecht, M. H., Kounaves, S. P., Quinn, R. C., et al. 2009, *Sci*, 325, 64
 Hilbig, R., & Wallenstein, R. 1981, *IJQE*, 17, 1566
 Hudson, R. L., & Moore, M. H. 2004, *Icar*, 172, 466
 Ibañez, D., Santidrian, A., Heras, A., Kalbáć, M., & Colina, A. 2015, *JPCC*, 119, 8191
 Improta, R., Santoro, F., & Blancafort, L. 2016, *ChRv*, 116, 3540
 Jones, B. M., & Kaiser, R. I. 2013, *JPCL*, 4, 1965
 Kaiser, R. I., Maity, S., & Jones, B. M. 2014, *PCCP*, 16, 3399
 Kaiser, R. I., & Maksyutenko, P. 2015, *JPCC*, 119, 14653
 Keresztszti, Á., & Góbi, S. 2014, *P&SS*, 103, 153
 Kim, Y. S., & Kaiser, R. I. 2010, *ApJ*, 725, 1002
 Kim, Y. S., Wo, K. P., Maity, S., Atreya, S. K., & Kaiser, R. I. 2013, *JACChS*, 135, 4910
 King, S. T., & Strope, J. H. 1971, *JChPh*, 54, 1289
 Lasne, J., Noblet, A., Szopa, C., et al. 2016, *AsBio*, 16, 977
 Leshin, L. A., Mahaffy, P. R., Webster, C. R., et al. 2013, *Sci*, 341, 1238937
 Levy, M., & Miller, S. L. 1998, *PNAS*, 95, 7933
 Lewis, R. J., Sr. (ed.) 2007, Hawley's Condensed Chemical Dictionary (15th ed.; Hoboken, NJ: Wiley), 779
 Lowenthal, M. S., Khanna, R. K., & Moore, M. H. 2002, *AcSpA*, 58, 73
 Maier, G., Eckwert, J., Bothur, A., Reisenaur, H. P., & Schmidt, C. 1996, *Liebigs Ann.*, 1996, 1041
 Maity, S., Kaiser, R. I., & Jones, B. M. 2014, *FaDi*, 168, 485
 Maksyutenko, P., Förstel, M., Crandall, P., et al. 2016, *CPL*, 658, 20
 Miller, F. A., & Wilkins, C. H. 1952, *AnaCh*, 24, 1253
 Miller, K. E., Eigenbrode, J. L., Freissinet, C., et al. 2016, *JGRE*, 121, 296
 Miller, S. L., & Cleaves, H. J. 2007, Systems Biology, Vol. 1 (1st ed.; New York: Oxford Univ. Press)
 Minaev, B. F., Shafranyosh, M. I., Svida, Y. Y., et al. 2014, *JChPh*, 140, 175101
 Ming, D. W., Archer, P. D., Glavin, D. P., et al. 2014, *Sci*, 343, 1245267
 Mohamed, T. A., Shabaan, I. A., Zoghaib, W. M., et al. 2009, *JMoSt*, 938, 263
 Molina-Cuberos, G. J., Stumpfner, W., Lammer, H., Kömle, N. I., & O'Brien, K. 2001, *Icar*, 154, 216
 Moores, J. E., & Schuerger, A. C. 2012, *JGRE*, 117, E08008
 Muñoz-Caro, G. M., Mateo-Martí, E., & Martínez-Frías, J. 2006, *Sensors*, 6, 688
 Nowak, M. J., Lapinski, L., Kwiatkowski, J. S., & Leszczyński, J. 1996, *JPCA*, 100, 3527
 Orgel, L. E. 2004, *OLEB*, 34, 361
 Oró, J., & Holzer, G. 1979, *JMolE*, 14, 153
 Parr, G. R., & Taylor, J. W. 1974, *IJMIP*, 14, 467
 Pavlov, A. A., Vasilyev, G., Ostryakov, V. M., Pavlov, A. K., & Mahaffy, P. 2012, *GeoRL*, 39, L13202
 Pearce, B. K. D., & Pudritz, R. E. 2016, *AsBio*, 16, 853
 Perun, S., Sobolewski, A. L., & Domcke, W. 2005, *CP*, 313, 107

- Pilling, S., Lago, A. F., Coutinho, L. H., et al. 2007, *Rapid Commun. Mass Spectrom.*, 21, 3646
- Poch, O., Jaber, M., Stalport, F., et al. 2015, *AsBio*, 15, 221
- Poch, O., Kaci, S., Stalport, F., Szopa, C., & Poll, P. 2014, *Icar*, 242, 50
- Raulin, F., Fonsalas, F., & Wolny, M. 1984, *OrLi*, 14, 151
- Rice, J. M., & Dudek, G. O. 1967, *JACS*, 89, 2719
- Roy, D., Najafian, K., & von Ragué Schleyer, P. 2007, *PNAS*, 104, 17272
- Ruscic, B., & Berkowitz, J. 1994, *JChPh*, 100, 4498
- Saïagh, K., Cloix, M., Fray, N., & Cottin, H. 2014, *P&SS*, 90, 90
- Schuerger, A. C., Clausen, C., & Britt, D. 2011, *Icar*, 213, 393
- Schwell, M., Jochims, H.-W., Baumgärtel, H., Dulieu, F., & Leach, S. 2006, *P&SS*, 54, 1073
- Seki, T., & Ikariya, T. 2009, *PCCP*, 11, 10073
- Shivak, J. N., & Pavlov, A. 2012, American Geophysical Union, Fall Meeting 2012, Abstract #P11F-07
- Smith, M. L., Claire, M. W., Catling, D. C., & Zahnle, K. J. 2014, *Icar*, 231, 51
- Stirling, A., Pápai, I., Mink, J., & Salahub, D. R. 1994, *JChPh*, 100, 2910
- Sutter, B., Ming, D. W., Boynton, W. V., et al. 2009, *LPICo*, 1502, 29
- Tarczay, G., Förstel, M., Maksyutenko, P., & Kaiser, R. I. 2016, *InCh*, 55, 8776
- ten Kate, I. L. 2010, *AsBio*, 10, 589
- Toner, J., Catling, D., & Light, B. 2014, *GeCoA*, 136, 142
- Tonkyn, R. G., Winniczek, J. W., & White, M. G. 1989, *CPL*, 164, 137
- Turner, A. M., Abplanalp, M. J., Chen, S. Y., et al. 2015, *PCCP*, 17, 27281
- Turner, A. M., Abplanalp, M. J., & Kaiser, R. I. 2016, *ApJ*, 820, 127
- Vandenbussche, B., Ehrenfreund, P., Boogert, A. C. A., et al. 1999, *A&A*, 346, L57
- Voet, A. B., & Schwartz, A. W. 1983, *Bioorg. Chem.*, 12, 8
- Watanabe, K., Matsunaga, F. M., & Sakai, H. 1967, *ApOpt*, 6, 391
- Wilson, E. H., Atreya, S. K., Kaiser, R. I., & Mahaffy, P. R. 2016, *JGRE*, 121, 1472
- Zheng, W., Jewitt, D., & Kaiser, R. I. 2006a, *ApJ*, 639, 534
- Zheng, W., Jewitt, D., & Kaiser, R. I. 2006b, *ApJ*, 648, 753